The last deglaciation in the Picos de Europa National Park (Cantabrian Mountains, Northern Spain)

Ana Moreno[1,2,3], Blas L. Valero-Garcés[2,3], Montserrat Jiménez-Sánchez[4], María José Domínguez-Cuesta[4], M. Pilar Mata[5], Ana Navas[6], Penélope González-Sampériz[2], Heather Stoll[4], Pedro Farias[4], Mario Morellón[2], J. Pablo Corella[2], and Mayte Rico[2]

[1]Limnological Research Center, University of Minnesota, 310 Pillsbury Drive SE, Minneapolis, MN 55455, USA. moren079@umn.edu

[2]Instituto Pirenaico de Ecología (CSIC), Avda. Montañana 1005, 50059 Zaragoza, Spain. amoreno@ipe.csic.es; blas@ipe.csic.es; pgonzal@ipe.csic.es; mayterico@ipe.csic.es; mariomm@ipe.csic.es; pablocorella@ipe.csic.es.

[3]Laboratorio Internacional de Cambio Global (LINCGlobal), Departamento de Ecología, Facultad de Ciencias Biológicas, PUC, Alameda 340, PC 6513677, Santiago, Chile

[4]Departamento de Geología, Universidad de Oviedo, C/ Arias de Velasco, s/n 33005 Oviedo, Spain. mjimenez@geol.uniovi.es; mjdominguez@geol.uniovi.es; hstoll@geol.uniovi.es; pfarias@geol.uniovi.es

[5]Departmento de Ciencias de la Tierra, Universidad de Cádiz. CASEM, E-11510, Cádiz, Spain. pilar.mata@uca.es.

[6]Estación Experimental de Aula Dei (CSIC), Apdo 202, 50080 Zaragoza, Spain. anavas@eead.csic.es

Abstract

A sedimentological and geochemical study of the Lago Enol sequence (Cantabrian Mountains, Northern Spain) together with detailed geomorphological mapping provides a first record of glacier evolution and climate change over the last 40,000 years in the Picos de Europa National Park. The Enol glacier retreated from its maximum extent prior to 40 kyr BP as demonstrated by the onset of proglacial lacustrine sedimentation in two glaciated depressions, the Comella Hollow to the north (before 40 kyrs BP) and the Lago Enol (before 38 kyrs BP). These results support previous evidence that the maximum extent of southern Europe glaciers occurred earlier than in northern Europe.

Alternation of homogeneous and laminated proglacial sediments during the glacier retreat illustrate a dynamic glacial evolution during the Oxygen Isotopic Stage (OIS) 3 (40 – 26 kyr BP). A slight warming is detected at 26 kyrs ago with the change from proglacial sediments (in a lake located in contact to the glacier) to glaciolacustrine sedimentation (in a non-contact or distal lake). Finally, the onset of organic-rich sediments took place at 18 kyrs ago. This last transition occurred in two phases similarly to the North Atlantic Last Termination suggesting a link between North Atlantic Deep Water formation oscillations and paleohydrological variability in the Cantabrian Mountains.

Keywords: Last deglaciation; geomorphological mapping; lake sedimentology; Picos de Europa National Park

1. Introduction

The sensitivity and rapid response of alpine glaciers to moisture and temperature fluctuations makes them a potentially excellent source of information on past climate changes (Ivy-Ochs *et al*., 2008). However, most of past geomorphologic evidence of glacial activity are erosive and difficult to date, and glacial deposits usually do not provide a continuous record and contain scarce terrestrial remains for radiocarbon dating, hampering accurate chronologies for reconstructing glacial evolution (Leonard and Reasoner, 1999). Thus, lacustrine sediments obtained from glacial lakes constitute an excellent archive to reconstruct long-term paleoenvironmental changes, usually providing high-resolution records of glacial erosion and runoff (Ohlendorf *et al*., 2003). In order to identify changes in climate and in the catchment area, different indicators measured in lacustrine sediments, such as biological proxies or sediment geochemistry, must be compared and analyzed in combination (eg. Lotter and Birks, 2003).

Particularly interesting for the understanding of alpine glacier progress and their response to climate are the mountains from southern Europe since there (Alps, Pyrenees, Vosgues) a different evolution took place during the last glacial cycle that remains unexplained (eg. Gillespie and Molnar, 1995; Guiter *et al.*, 2005; Hughes and Woodward, 2008). Thus, in the Pyrenees it has been documented that the maximum ice extension of the last Pleistocene glacial cycle occurred earlier than the global last glacial

maximum (LGM) of Marine Isotope Stage 2 (MIS 2) (Florineth and Schlüchter, 2000; García-Ruíz *et al.*, 2003; Jalut *et al.*, 1992; Pallàs *et al.*, 2006). Geomorphological and sedimentological data from pro-glacial lakes show stable ice positions until about 30,000 cal yr BP when the onset of the ice retreat started, as shown from peatbog records in the Central Pyrenees (González-Sampériz *et al*., 2006). The cessation of glaciolacustrine sedimentation at high altitude sites indicates that glaciers were essentially confined to cirques in the Pyrenees after 18,000 cal yr BP (see review in Delmas *et al*., 2008).

The first research developed in the Cantabrian Mountains (Northwestern Iberian Peninsula) has shed some light on glacial history in the region (Jiménez Sánchez and Farias, 2002) which appears to be coherent with the chronology previously established for the Pyrenees (Jalut *et al*., 1992). However, better dates and more continuous records are necessary since only few pre-Holocene absolute ages have been reported until now in Redes Natural Park and Comeya hollow (Jiménez Sánchez and Farias, 2002; Jiménez Sánchez *et al.*, 2002). The Picos de Europa National Park (PENP), located in the eastern Cantabrian Mountains, represents an outstanding mountain ecosystem due to its geological and biological features, and particularly the activity and effects of glacial and periglacial processes in landscape evolution, vegetation composition and distribution (Marquínez and Adrados, 2000). The PENP lies in a key location to reconstruct the paleoenvironmental history since last deglaciation thanks to the proximity of northern Iberian Peninsula to the southern position of the North Atlantic Polar Front during the last glacial maximum (LGM) (Ruddiman and McIntyre, 1981). In that region, although some marine cores have been recently studied (Naughton *et al*., 2007), terrestrial records from lakes or caves are still scarce and mostly span only the Holocene period (Domínguez-Villar *et al.*, 2008) The PENP contains one of the deepest lakes in the Cantabrian Range (Lago Enol) thus providing an opportunity to unravel the glacial evolution and associated climate changes in the area. The main goal of this study is to provide a pluridisciplinar analysis of past environmental changes in the PENP, based on the Enol lacustrine sequence and the glacial deposits associated. In this paper, we present a multi-proxy reconstruction, combining sedimentological and geochemical indicators as evidence of the paleolimnological evolution on Lago Enol during the last 40,000 yr and supported by a detailed geomorphological framework that resolves the

timing and spatial extent of main deglaciation phases in this area of the Cantabrian Mountains.

2. Present-day climate and geographical setting

2.1. Geological and geographical context

The Picos de Europa Mountains are located in the eastern Cantabrian Mountain Range (NW Spain). The range shows the highest elevations in the south (up to 2600 m asl) and progressively descends towards the Cantabrian Coast in the north. The present landscape of the Cantabrian Mountains results from a structural relief created by a monoclinal flexure and associated reverse faults with an E-W trend during the Alpine Orogeny (Alonso *et al*. 1996; Marquínez 1992). The alpine relief was eroded by rivers flowing S to N, that generated deep and steep valleys as the Cares Gorge where slope processes are active and rockfall deposits common. The most outstanding features of the landscape are glacial and karstic landforms which have been widely described in this area from the beginning of the last century, although periglacial and gravity processes have been also reported (Obermaier, 1914; Hernández Pacheco, 1914; Miotke, 1968; Smart, 1986; Alonso, 1992, 1998; Flor, 2004; Marquínez and Adrados, 2000; Farias *et al*. 1990, 1996; Gale and Hoare, 1997; Jiménez-Sánchez and Farias 2002, Santos Alonso and Marquínez, 2005). Lago Enol and Lago Ercina (Fig. 1) are respectively located at 1,050 and 1,110 m asl over Carboniferous bedrock, mainly composed of limestone, (Picos de Europa and Valdeteja Formations), as well as siliciclastic materials (Amieva Series), all of them affected by faults trending NW-SE and E-W. The relationships between the lakes and the Carboniferous bedrock are not well established, since Quaternary sediments, mainly composed by till and rockfall deposits, obscure the contact with the Paleozoic Formations.

Lago Enol (43º16'N, 4º59'W, 1070 m asl; Fig.1) is located in the Western Massif of the Picos de Europa Mountains. From a geological point of view, this area is located in the Eastern part of the Cantabrian Zone and following Marquínez (1989) and Bahamonde *et al*. (2007), includes three groups of Paleozoic rocks: Cambro-Ordovician rocks (mainly represented by the Lancara Limestone, the Oville Sandstone and the Barrios Quartzite), Carboniferous limestones, (Alba, Barcaliente, Valdeteja and Picos de Europa

Formations) and Carboniferous detrital formations, mainly composed by lutites. Between Lago Enol and Lago Ercina a 70 m maximum height well-preserved moraine occurs (Entrelagos Peak, 1,175 m asl). Lago Ercina (Fig. 1) is now artificially dammed and it is being progressively infilled by sediments. Lago Enol is bounded to the north by calcareous outcrops of the Valdeteja limestone. An E-W trending fault with a 200 m height scarp separates the Lago Enol area from the Comeya hollow, a basin of smooth topography with a surface of 1,2 km^2 (Fig. 1). The Comeya hollow is partly modeled in limestones of Picos de Europa Formation as well and in the siliciclastics rocks of the Amieva Series. The northern boundary with the Barrios Quartzite Formation is also tectonic. The Comeya hollow was interpreted by Obermaier (1914) as a glacial basin over-excavated prior to the last glaciation. More recent studies suggest a karstic-tectonic and glacial origin as poljé delimited by faults trending E-W and affected by glacial activity (Farias *et al*., 1990, 1996).

2.2. Previous research on glacial landscape history

The diversity of the lithological composition of the bedrock, the interaction between karstic and glacial processes, the superposition of karstic features to glacial erosion features as well as the probable superposition of glacial erosion features belonging to different glacial episodes, contribute to the complexity of the landscape morphology in the PENP. Also, the scarcity of well preserved till deposits restricts the establishment of glacial stabilization phases as well as the position of glacial fronts. Glacial cirques, glacial valleys, glacio-karstic hollows, ice-polished surfaces and till deposits in the Lago Enol area have been reported and described in several previous studies (Obermaier, 1914; Miotke, 1968; Smart, 1986; Alonso, 1992, 1998; Flor, 2004; Marquínez and Adrados, 2000). Based on geomorphological studies, several hypotheses about ice flow patterns (Alonso, 1998; Flor, 2004), and even the reconstruction of the glacier morphology during the LGM (Marquínez *et al*., 1990; Marquínez and Adrados, 2000) have been proposed. As described by Alonso (1998), in the northern slope of the western Massif, the only evidence of the position of glacier fronts are those corresponding to the frontal moraines of Enol and Ercina and the lateral moraines of Belbín (East of Lago Ercina) and Pandecarmen (SW of Lago Enol), located at about 1000 m altitude. In the south of the Massif, other moraines at 1150 and 1220 m asl would have probably defined glacial fronts. In addition, the best example of a glacial

valley is located at the southwest of Lago Enol (Fig. 2). Glacial cirques and glaciokarstic hollows (Smart, 1986) reaching altitudes higher than 2400 m asl (Jou Santu, Peñasanta Peak, Torre de Santa María Peak) defined the head of the glaciers, while the bottom of glacial cirques would permit the inference of an altitude of 1550 m for the snow line during the maximum extent of the glaciers (Marquínez *et al*. 1990; Marquínez and Adrados, 2000).

Therefore, the geomorphological evidence reported until now can be grouped in two types of glacial indications: 1) the well-preserved glacial features (cirques, moraines and the Enol valley glacier), that have been useful to define flow patterns, as well as glacier fronts around 1000 m in the North of the massif and 2) the poorly preserved glacial features, as polished surfaces or slope scarps which are partially-masked by karstic and gravitational processes, that could be indicative of glacial fronts reaching altitudes lower than 1000 m.

The different reconstructions of the glacial history of the Picos de Europa can be explained by difficulties in recognizing and interpreting glacial features. However, in spite of the different models, most of the studies agree that glacial ice would have covered the highest areas of the Western Massif and flowed in a radial pattern with a source area in the cirques and glaciokarstic hollows located in Santa María and Peñasanta Peaks, higher than 2400 m asl. Only Flor (2004) have described glacial evidence in the NW part of the massif. The predominating flow directions (SE to NW) would have been controlled by the previous structure (Alonso, 1998). Glacial fronts are assumed to have reached altitudes between 700-800 m and even 500 m asl (Marquínez and Adrados, 2000). However, no glacial deposits have been directly dated in the PENP. Although the possibility of former glaciations was considered in early studies (Obermaier, 1914; Gale and Hoare, 1997), recent surveys indicate that glacial activity during the last glaciation would have destroyed evidence of former glaciations (Marquínez and Adrados, 2000). The only available radiometric dating comes from the deposits in the Comeya hollow, located to the NW of Lago Enol and Lago Ercina (Fig. 1). Two cores with a length of 42.5 m (S'1) and 56.7 m (S'2) showed a sedimentary sequence composed of colluvial, torrential and lacustrine facies (Farias *et al*. 1996)**.** The development of a proglacial lake in the Comeya hollow is probably a result of the ablation of the Enol-Ercina glacier with its front located at 1030 m, where the terminal

moraines of Lago Ercina and Lago Enol occur (Fig. 2). Lacustrine organic-rich sediments at a depth of 35.5 m were dated to 40,480 ± 820 yr BP (68% range calBP: 43,232 – 45,003), and interpreted as synchronous with the presence of the glacier front in Enol (Jiménez-Sánchez and Farias, 2002, Jiménez-Sánchez *et al*. 2002).

2.3. Present-day setting: climate, vegetation and hydrology

The study area is characterized today by temperate oceanic climate, i.e., high annual precipitation (above 1000 mm) due to the proximity to the ocean. Winters are mild and summers are cool with a annual temperature of ca. 13°C. Rainfall mostly occurs in winter, associated with mid-latitude storms from the Atlantic Ocean. As in other areas of northern Spain, much of the present day climate variability in this region on a decadal timescale has been linked to the North Atlantic Oscillation (NAO; Trigo *et al*., 2004).

The region is located within the phytogeographical Eurosiberian region. The mentioned mild-humid climatic characteristics favour the development of dense deciduous forest formations, mainly in oceanic wind slopes where, in addition, peatlands are abundant. The forested areas are dominated by *Quercus robur* with *Betula alba, Corylus avellana, Fraxinus excelsior, Alnus glutinosa,* or *Acer pseudoplatanus* together with scrub Ericaceae and Fabaceae extensions within a Poaceae herbaceous composition (Peinado-Lorca and Rivas-Martínez, 1987). The Lago Enol margins are occupied by a vegetation belt of Poaceae, Fabaceae, Asteraceae and Cyperace species.

Lake Enol has a water surface area of 12.2 ha and a maximum depth of 22 m. The small watershed (1.5 km^2) is located over Carboniferous formations: limestones in the north and south borders (Valdeteja and Picos de Europa Formations) and lutite and sandstone (Amieva Series) elsewhere. The Picos de Europa Formation constitutes the most important regional karstic aquifer in the area of the National Park and is characterized by preferential groundwater flow through main structural directions (N100º-120º) (Meléndez Asensio *et al*., 2002). This area was glaciated with predominantly north to northeast ice flow (Marquínez and Adrados, 2000). Thus, Lago Enol was overexcavated by a glacier coming from the southwest, although probably previous karstic processes could have been involved in the origin of the basin. The present day bathymetry with a

steep south margin, deeper area in the south and central areas, a low gradient north margin with a small platform is the result of glacial erosion of the bedrock and deposition of the basal till and moraine.

The lake is fed by laminar (unconfined) runoff and no permanent inlet exists at present. An outlet in the northeast border drains water to the Comeya hollow (Fig. 1). Groundwater inputs and outputs and evaporation are controlling the hydrological balance of Lago Enol. Although there are no available groundwater and lake level data to calculate the hydrological balance in the lake, the response of the system to precipitation is assumed to be relatively rapid (Meléndez Asensio *et al*., 2002).

Vertical hydrographic profiles in May 2004 revealed thermal stratification with a thermocline located at 10 m depth and only modest changes of electrical conductivity and pH through the water column were observed (pH = 7.7 to 8.2). Lake waters are oligotrophic (total phosphorus 8 μg l^{-1}(Velasco *et al*., 1999), moderately hard (alkalinity 2.4 meq l^{-1}; 29 mg Ca l^{-1}) and carbonate and calcium - rich ($[HCO_3^{2-}] > [Ca^{2+}] > [SO_4^{2-}]$) with a conductivity of 202 μS cm^{-1}. Calculations of mineral speciation indicated that present-day bottom water is undersaturated in calcite, at least seasonally. Given current measured bottom water chemistry, temperature fluctuations are not enough to change the saturation state (with a temperature of 12ºC, calcite will still be undersaturated). Dissolved CO_2 in bottom waters, calculated from alkalinity and pH measurements, is in excess of atmospheric values (pCO_2 = 1500μatm) suggesting that organic matter decomposition contributes to the observed calcite undersaturation. Modern sediments contain organic matter (≈8%), carbonate (≈9%) and silicates. Carbonate fraction is mostly detrital, with a small component of charophyte and gastropod remains in littoral zones. The presence of calcite in the lake sediments from the deeper areas indicates that dissolution processes are not intense enough to destroy all the carbonate. Preservation potential for carbonates in Enol deeper areas would increase with (1) physical mixing processes leading to higher degassing of bottom water potential and/or (2) an increase in alkalinity produced by higher dissolution of surrounding limestone as a consequence of more acidic water.

3. Material and methods

Field work included intensive geomorphological mapping and a lake coring expedition. Till deposits were mapped at a 1:10,000 scale in an area of 5.4 km^2 in the surroundings of Lago Enol by field work and photointerpretation. These deposits can be recognized as an accumulation of sub-angulous blocks and gravels embedded in a clayey matrix without any sedimentary structure. A Digital Elevation Model of the area and different derived Digital Terrain Models (slope and aspect) were obtained from the digital topographical information published by the Asturias Government at a scale of 1:5000. The geomorphological information was digitized and transferred to a Geographical Information System. The presence of polished surfaces, moraine ridges and glaciated valleys (Fig. 2) were used to estimate the ice flow patterns as well as its approximate thickness.

The two selected cores for this study were retrieved from the deepest central area of Lago Enol (ENO04-1D-1K, 588 cm long) and close to the frontal moraine (ENO04-2A-1K, 541 cm long) (Fig. 1 and 2) in the spring of 2004 with a modified Kullenberg piston coring platform from the Limnological Research Center (LRC), University of Minnesota (USA). Due to the coring procedures, several cm were lost at the top of both cores. Physical properties (including magnetic susceptibility and Gamma Ray Attenuation – GRA - bulk density) were measured every cm with a standard GEOTEK Multi-Sensor Core Logger (MSCL) at the LRC. Results are reported as instrumental units. The cores were split, imaged with a DMT core scanner and analyzed for magnetic susceptibility every 0.5 cm with a high resolution point sensor (MS2E) mounted in a GEOTEK MSCL-XYZ. The Lightness (L*) parameter was obtained derived from digital image of the core lithologies following the LRC procedures (http://lrc.geo.umn.edu).

Sedimentary facies were defined by macroscopic visual description including color, grain-size, sedimentary structures, fossil content, and by microscopic smear slide observations (Schnurrenberger *et al.*, 2003) (Table 1; Fig. 3). Up to 14 samples distributed along the core and representing the whole sedimentological variability were analyzed for grain-size distributions by a Coulter LS230 after removing the organic content by H_2O_2 and using a dispersant agent to disaggregate the samples (Table 1). In core ENO04-1D-1K, whole sediment mineralogy was characterized by X-ray diffraction

with a Bruker D8-Advance diffractometer every 5 cm and relative mineral abundance was determined using peak intensity following the procedures described in Chung (1974). Both cores were sampled every 5 cm for organic matter and carbonate content. Total Carbon (TC) and Total Inorganic Carbon (TIC) contents were determined by a UIC model 5011 CO_2 Coulometer at the LRC and Total Organic Carbon (TOC) was calculated by subtraction. X-Ray Fluorescence (XRF) data used in this study were produced by the ITRAX XRF core scanner from the Large Lakes Observatory (Duluth) of the University of Minnesota (USA) using 30 seconds count time, 30 kV X-ray voltage, an X-ray current of 20 mA, a step size from 1 cm to 2 mm and a Molybdenum anode x-ray tube to obtain significant data of the following elements: Si, K, Ca, Ti, V, Cr, Mn, Fe, Rb, Sr, Y, Zr, Ba, Pb (Fig. 4A). Element concentrations are not directly available by the XRF measurements and the installed processing software. In order to determine the concentration of some key elements, a total of 37 samples were digested with HF (48%) in a microwave (Milestone 1200 mls) and analyzed for major-element composition by atomic emission spectrometry using inductively coupled plasma (ICP-OES) with solid-state detector (Perkin Elmer Optima 3200 DV). As plotted in Fig. 4B, there is a high correlation between ICP-OES and XRF-scanner data for some elements (Ca, Fe, Mn, Cr, K). However, some elements were not obtained by ICP-OES technique (V, Ti, Si, Zr) and some others, usually not well-detected by the XRF scanner, present a low correlation (Ba, Pb, Al – not shown). Consequently, and consistent with most published studies (e.g. Moreno *et al.*, 2007; Moreno *et al.*, 2008), the original XRF core scanner data are expressed in cps and considered semi-quantitative data. X-ray radiographs were obtained with the same ITRAX core scanner using 60 kV X-ray voltage and 60mA of current intensity.

Statistical treatment of the whole dataset (17 variables and 579 cases) was carried out using the Multi-Variate Statistical Package (MVSP 3.1) (Fig. 5) including Correlation Analyses (CA) and Principal Component Analyses (PCA) with the main obtained data (XRF, TIC, TOC, MS and L*). All the variables were linearly interpolated with a regular spacing of 1 cm in order to retain the maximum information from the XRF, and were normalized in order to avoid problems arising from their different orders of magnitude. Due to the discontinuous character of grain-size and XRD data, they are not included in these analyses.

Twenty-two AMS ^{14}C dates from the Lago Enol sediments (cores 1D and 2A) were obtained from bulk organic matter, plant remains and charcoal samples (Table 2). Seventeen dates have been converted into calendar ages by the CALIB 5.0.2 software that uses the most updated data set (INTCAL04; Reimer *et al*., 2004). The median of the 1σ probability interval was selected for these dates resulting in errors of ±70 yr (in average) in the obtained calendar ages. CALPAL software was used for the five oldest dates, since they were outside the limits of previous calibration. The calibration of ^{14}C ages prior 25,000 yr BP is difficult because of the poor knowledge on the quantitative production of cosmogenic ^{14}C along oxygen isotopic stage 3 (OIS 3), the presence of various rises and plateaux and the extremely low residual concentration of ^{14}C in such samples (Bard *et al*., 2004). The CALPAL software combines the different available approaches to calibrate ^{14}C ages, such as speleothems, corals or varved sediments data (http://www.calpal.de) but the final errors are still large (approximately ± 800 yr). Therefore, the calibration difficulties for the oldest dates in this sequence together with the scarcity of organic remains, remained an obstacle to a good chronological framework for the lowermost unit of the sequence (Fig. 6). Those oldest dates must be then considered as maximum dates. Finally, the chronology was constructed by interpolating the radiocarbon dates listed in Table 2 using a generalized mixed-effect regression (Heegaard *et al*., 2005).

4. Results

4.1. Cores sedimentological and geochemical description and interpretation

4.1.1. Sedimentary facies and mineralogy

Two cores are used to characterize the Lago Enol sedimentary sequence: core 1D, located in the centre of the lake at 21.5 m water depth, and core 2A, recovered from a shallower area, close to the frontal moraine and at 12.5 m water depth (Fig. 2). The complete lacustrine sequence was not recovered in the core of the deepest zone. In the shallower core, glacial till facies were reached at the base of core 2A (Fig. 3) indicating that the 6 meter long sequence constitutes the entire sedimentary sequence since the lake was formed after the glacier retreat. The sediments consist of banded to finely laminated silts with variable carbonate content (mostly coarse-silt detrital calcites),

siliciclastic minerals (quartz, clays, feldspars) and terrestrial organic matter. Five main sedimentary facies were identified after integration of visual description, grain size, microscopic observations and mineralogical and geochemical composition (Table 1).

Facies 1 and 2 are banded, silts to coarse silts, calcite-rich sediments, with high percentages of organic matter. Particularly in Facies 2 mm-thick layers appear which are mostly composed of macrophyte remains (Fig. 3). Facies 1 represents deposition in the off-shore areas of the lake, where clastic and some endogenic (carbonate from the littoral platform) particles accumulate. Facies 2 marks periods of higher energy (floods) when macrophytes growing in the littoral areas are reworked and transported to deeper environments. Facies 1 and 2 correspond to deposition in Lago Enol during non-glaciated periods. Facies 3 and 4 are finer (clay to fine silts), siliciclastic-rich and only occur in the lower part of the sequence, except for a thin interval of Facies 3 in core 1D (160-180 cm).

Facies 3 consists of dark grey silty clays, massive or slightly banded with very low organic matter (TOC remains below 2%). The clay fraction contains phyllosilicates (illite, muscovite), quartz and feldspars while coarser particles are composed of quartz. Facies 4 groups light grey and brown massive and laminated facies with some carbonate and almost absent organic matter (TOC values among 0.2 and 0.6%). Compositional and textural criteria define three subfacies: i) 4a is composed of dark brown to grey fine silt and clays, banded to faintly laminated, ii) 4b is composed of finely laminated (< 1 mm thick) with carbonate content up to 4 % TIC, iii) 4c groups massive to faintly laminated, light grey, carbonate-rich facies. A closer inspection reveals that lamination in subfacies 4b is composed of three laminae: (a) gray, fine grained, clay – rich, (b) light brown with 10-15% of silty calcitic crystals and (c) brown lamina made of coarser (silt fraction) calcite particles with some quartz and feldspar but without fine clay matrix. Rhythms are composed of laminae type “a” and “b”; sandy laminae “c” are less frequent. Subfacies 4b occur in two intervals in core 1D (400-500 cm depth and 340-360 cm) and in several intervals in core 2A (450-550 cm). Finally, Facies 5 is a 2 cm thick carbonate sandy layer with abundant shell fragments in core 2A at 315 cm depth. It represents the littoral deposition in the carbonate lacustrine shelf.

4.1.2. Physical properties

Magnetic susceptibility of Lago Enol sediments is highly variable (8-30 SI) (Fig. 3). In general, lower values are reached during the glacial interval, except in the rhythmites (Subfacies 4b) and coarser, carbonate –rich facies (Subfacies 4c), while higher values appeared during the Holocene. The association of MS values with magnetic minerals is not clear in Enol sediments because the low concentration of those minerals precludes their determination by XRD and they do not appear in smear slide observations. However, the simultaneous increase of MS and TOC may point to an association, likely related to the presence of S-rich minerals that are usually abundant when organic content is high. In Lago Enol sediments the MS can be also related to grain-size, water content and density of the sediment (Arnaud *et al*., 2005). Thus, Facies 1 and 2 with lower density, higher carbonate content and coarser grain size show higher values of MS (Fig. 3). An exception to this pattern occurs from 320-340 cm where the MS peaks are clearly associated with increases of Mn and Fe (Fig. 4) pointing to the presence of pyrite or other redox-related elements that usually have a magnetic signal (Aguilar and Nealson, 1998; Blum, 1997). Bulk density was measured along sediment cores 1D and 2A (Fig. 3) and clearly marks the change from glacial sediments with high density values likely due to the small grain-size of clay particles compared to coarser Holocene sediments. This is confirmed by the grain-size results obtained from several samples distributed throughout core 1D (Table 1). Finally, the lightness of these sediments is represented in Fig. 3. During the lower three meters of the sequence, this color parameter seems to correlate to the carbonate content of the sediments (light colors, high L* values) but to the organic content during the uppermost 2 meters (dark colors, low L*).

4.1.3. Organic and inorganic carbon content

Due to the absence of other carbonate minerals as demonstrated by the XRD analyses, total inorganic carbon can be used as an indicator of calcite content (Fig. 3). Organic matter mostly occurs as large fragments of terrestrial and littoral plant remains in mm-thick layers along the Holocene (Facies 2). TOC and TIC percentages show similar trends: carbonate and organic carbon increase sharply in both cores (1D and 2A) at 200 cm depth (8-10% for TOC and 6% for TIC, what means up to 50% of calcite assuming all inorganic carbon deriving from that mineral) while lower values are characteristic of

the lower four meters (Fig. 3). In fact, the TOC content remains around 0.3 % until 300 cm depth when it starts to increase gradually to finally reach higher values at 200 cm depth. The TIC content in glacial sediments, although close to 0% for most of the interval, shows two significant increases parallel to higher values of MS and density (320-340 cm in core 1D; 340-370 cm in core 2A) (Fig. 3). Observations of smear slides from both intervals demonstrate the presence of carbonate, although in finer grain-size than during the Holocene (Table 1) and in lower amount (TIC values of 6-8% during the Holocene *vs* 2-3% during those two intervals, Fig. 3).

4.1.4. Major and trace element composition

The ITRAX XRF Core Scanner provided a high-resolution record of geochemical variations and the x-ray radiograph for the Lago Enol composite sequence (Fig. 4A). The density contrasts shown by the radiograph indicate the presence of organic-rich layers by lighter colors (less dense sediments, Facies 2) and of clay-rich facies by darker layers (denser sediments, Facies 4) (Fig. 4A). Regarding the geochemical composition of Lago Enol sequence, we observe a reverse pattern between Ca and the other elements (Si, K, Ti, V, Cr, Mn, Fe, Rb, Sr and Zr) along the whole records. Ca peaks at the top of the sequence and decreases downwards while Si, K, Ti, V, Cr, Mn, Fe, Rb, Sr and Zr display the opposite trend. Only Sr correlates to Ca during some short intervals (i.e. 400-500 cm). Some of the elemental profiles are replicated by analyzing several samples by ICP-OES along the sequence with the main aim of evaluating the observed changes and check the real concentrations for some elements (K, Ca, Cr, Mn, Fe; Fig. 4B). Thus, we observe a good correlation between the data measured by both geochemical techniques. The geochemical pattern, together with the information provided by the TIC and TOC % (see above), clearly indicates a dominance of clay-rich sediments for the lowermost sediments and of carbonate and organic-rich sediments towards the top of the sequence thus pointing to distinct changes in the depositional environment after the last glacial period.

4.2. Sedimentary units and core correlation

The sedimentary facies, magnetic susceptibility and lightness values, TIC and TOC percentages and the geochemical composition (XRF) identify three units in both cores

1D and 2A (Fig. 3). Basal Unit 3 is composed of laminated proglacial sediments (Facies 4) characterized by low MS, high density and lighter colors. In the deeper core (core ENO04-1D-1K) the lowermost part of the core, Unit 3, can be divided into three subunits based on lamination type and carbonate content. Subunit 3A is composed of banded to faintly laminated subfacies 4a with a calcite-rich intercalation of subfacies 4c (340-350 cm). Subunit 3B is relatively coarser, finely laminated (rhythmites) and contains calcite (up to 4 % TIC) in the silt fraction (subfacies 4b). This subunit is also characterized by the increase of Sr. In the shallower areas (core ENO04-2A-1K) Unit 3 is thinner (200 cm) but complete since the core reached the basal glacial till (Fig. 3). It is composed by a basal subunit with alternating decimeter- thick intervals of subfacies 4a and 4b. Without a chronological control, it is likely that this unit represent both subunits 3C and 3B in core 1D. The upper part, which could correlate with subunit 3A in core 1D, is composed of subfacies 4a at the base and subfacies 4c at the top.

Unit 2 is characterized by slightly higher MS and lower L* and density compare to Unit 3. It is formed by massive, non-carbonate, and low organic matter content Facies 3 in both cores (Fig. 3). The thickness of this unit in the littoral areas is greatly reduced, likely due to erosive processes as the nature of the lower boundary suggests. The upper boundary of Unit 2 is characterized by a 2 cm-thick layer made of shell fragments, indicative of the transgression of littoral, high bioproductivity post-glacial environments. Dates at the boundary between Unit 2 and 1 in the littoral core (Fig. 3) indicate a clear hiatus probably representing a sharp decrease in lake level.

The base of Unit 1 in core ENO04-1D contains several evidence of gravitational processes: i) sharp lithological boundaries at 200, 185 and 120 cm, ii) slightly tilted lamina from 140 to 120 cm, iii) a repetition of a complete sediment interval: the 185 to 165 cm interval corresponds to the 215 to 200 cm interval. Based on the stratigraphic and lithological evidence two sediment slides can be inferred with minimal internal deformation between 120 and 200 cm depth. The ^{14}C ages of this interval (Table 2 and Fig. 3) confirm the occurrence of these slides involving Lateglacial and early Holocene sediment. The age of the slide is constrained by the age of the top scar surface (120 cm) at about 9 ka (Fig 3). In addition to the sedimentological and chronological evidence, the detected slides are also observed as sharp changes in the geochemical composition (Fig. 4A). Thus, at the base of Unit 1 the sharp increase of Ca and decrease of the other

elements supports the erosive nature of this contact identified by the sedimentological description as the basal scar of a sediment slide. Sediments between 165-180 cm (Facies 3) are characterized by very low Ca and higher values of Si, K, Ti, V, Cr, Fe, Rb, Sr and Zr, similar to Unit 2 sediments, thus confirming the repetition of an interval of the sequence (Fig. 4A). Finally, from 120 cm upwards, above the slide interval, higher values of Ca coincide again with the lowest values of the siliciclastic elements.

Finally, the uppermost part of Unit 1, characterized by high values of MS and minimum density, represents post-glacial sediments and is composed of an alternating sequence of Facies 1 and 2. The dominance of Facies 1 indicates a continuous supply of detrital calcite punctuated by flooding episodes responsible for deposition of Facies 2. Unit 1 is thicker in the littoral zone, indicating a higher productivity and sediment delivery in these environments.

4.3. Correlation Analyses (CA) and Principal Component Analyses (PCA)

In order to objectively describe the main variance in the dataset using only a few factors and confirm the patterns observed previously by the downcore variation of the different proxies used in this study, a statistical treatment, based on correlation and principal component analyses was carried out.

4.3.1. Correlation analyses.

Ca displays a significant, but negative correlation with all other elements and positive correlation with MS (0.399), TIC (0.958) and TOC (0.785) (Table 3). Similarly, MS is negatively correlated with siliciclastic elements and positive with the percentage of TOC (0.486) thus supporting a relationship between flood layers (reworked plant remains) and higher MS. Manganese is the only element that does not show any correlation with the other variables, suggesting a different origin for this element, likely related to redox variations (Aguilar and Nealson, 1998). From the calculated correlations among the other elements, two different groups showing high correlation between the elements can be observed: (1) Si, K, Ti, Fe, Rb, Sr, V, Cr and (2) Zr, Pb, Ba.

4.3.2. Principal Component Analyses.

Principal Component Analysis (PCA) was carried out using a dataset of 17 variables and 579 cases to objectively describe the main variance using only a few factors and confirm the patterns observed previously using correlation analyses. The first two eigenvectors accounted for 81.37 % of the total variance (Table 4a). The first eigenvector represented 67.43 % of the total variance, and this eigenvector was controlled mainly by Ca, TIC, TOC and MS at the negative end and all the other light and heavy elements at the positive end (Fig. 5, Table 4b). On the other hand, the second eigenvector accounted for 13.94 % of the total variance, and was controlled by the opposition of Mn (positive end, charged 0.445) and Zr (negative end, charged -0.411) (Table 4b). The other variables, although not very significant in the second eigenvector, are organized as follows: L*, Si, Ca, Sr, TIC with Mn and Ba, Pb, Cr, TOC, MS and V with Zr (Fig. 5, Table 4b). The remaining eigenvectors defined by the PCA (Table 4a) were not taken into account to interpret the geochemical variability given that they accounted for very low percentages of the total variance.

The PCA analyses confirm a clear opposite pattern between carbonates (Ca, TIC) and organic matter (TOC and to some extent, MS), on one hand, respect to the rest of the elements that are associated with the clay fraction, on the other hand (Fig. 5). Not so evident is the interpretation of the second eigenvector that, due to the opposition of Mn and Zr may be interpreted as a redox signal (Eusterhues *et al.*, 2005; Hamilton-Taylor *et al.*, 2005; Morford and Emerson, 1999) but other processes such as the presence of carbonates including traces of Mn or Sr (although neither aragonite nor rhodochrosite was observed by XRD) may be playing a role in this second eigenvector. Further analyses of the minerals by SEM would be necessary to confirm the presence or absence of other carbonatic mineral phases.

4.4.- Chronological model

The age model of the Lago Enol sequence was constructed after taking into account three significant difficulties: (1) the possible hard-water effect due to dating bulk sediment samples in a carbonate-rich catchment area, (2) the presence of slides in Unit 1 and (3) the calibration of ages older than 25,000 yrs BP in Unit 3. Regarding the first

issue, the fact that two dates obtained from contiguous samples (one from bulk sediment at 183 cm and one from plant remains at 182 cm, Table 2) gave the same result gives us some confidence about the low influence of the hard-water effect.

The presence of older sediments overlying younger sediments as a consequence of a sediment slide in Unit 1 forces to subtract the "outsider" interval from the sequence and build an independent chronological framework for those sediments. Finally, those sediments were integrated in the age-depth model for the whole sequence (Fig. 6). This was possible since the extent of the slide is well-defined by sedimentological and geochemical characteristics (Fig. 3 and 4) and framed between the top of the tilted layers (for the uppermost part of the interval) and an erosive surface (for the base). The gravitational slide occurred between ca. 9800 cal yrs BP (age of the youngest sediments affected by the slide) and 9300 cal yrs BP (calculated age for the oldest sediments overlying the slide, according to our model). Although the presence of slides in the record complicates the reconstruction of the sediment sequence, the clear identification of the slides boundaries, the non-deformation of the sediments within the slides (not folded or disturbed, see core image in Fig. 3) and the good chronological control of the sediment both in the slides and in the original sequence allowed a detailed reconstruction of the sediment sequence in Enol.

To date the base of Enol sequence we have to consider the five dates obtained for Unit 3 in cores 1D and 2A (between 37,030 and 41,140 cal kyrs BP) that are not in rigorous stratigraphic order (Table 2). This problem is likely a consequence of the high error inherent to the dating and calibration of old sediments by ^{14}C (Bard *et al*. 2004) and, possibly, to the fact that we had to date bulk sediment due to the lack of organic macrorests remains. On the other hand, the presence of fossil carbon in the surrounding lithologies can be ruled out (Bahamonde *et al*., 2007). The five dates from Unit 3 were then averaged to get a basal age and construct the age model accordingly. Doing that, the first proglacial sediments were found in Enol cores at 38,300 cal yrs BP, and are coherent with the onset of lacustrine sedimentation in Comeya Hollow around 43,230 – 45,000 cal yr BP. The chronology for the lowest two meters of Lago Enol sequence is, however, imprecise and further interpretations will be taken with caution.

Finally, the chronology was constructed by interpolating the radiocarbon dates listed in Table 2 using a generalized mixed-effect regression (Heegaard *et al*., 2005). With the chronological model obtained, a variable sedimentation rate is observed throughout the sequence (Fig. 6). Unit 3, corresponding to OIS3, shows the highest linear sedimentation rate in the sequence (LSR=24 cm/kyr) coherently with its proglacial and laminated character. Unit 2, that includes last part of OIS3, the LGM and what has been called the "Mystery Interval" (Denton *et al*., 2006), was deposited very slowly (9.4 cm/kyr). The Mystery Interval matches the first phase of last deglaciation (18.5 to 14.6 kyr) and corresponds to low boreal (north) summer and high austral (south) summer insolation, to low temperatures in Greenland (HE1) but to sea level rise (Denton *et al*., 2005). In the Lago Enol record, that interval corresponds to the lowest LSR of the whole sequence (3 cm/kyr). Unit 1 can be separated in two intervals regarding LSR values: first one which embraces the Bølling-Allerød and the Younger Dryas and second one covering the Holocene (Fig. 6). Although the onset of the Bølling-Allerød would represent an increase in the amount of erodible material in the catchment, the still very low LSR (3 cm/kry) and the fact that it corresponds to one of the slide scars (Fig. 3) leads us to hypothesize that the absence of some material due to the erosive action of the slide is possible. However, we did not detect any erosive surface to clearly evidence the hiatus. Relatively high sedimentation rates resume in the Holocene (12.8 cm/kyr).

5. Glacial and environmental evolution reconstructed since last deglaciation

In the surroundings of Lago Enol and Lago Ercina, till deposits have been mapped at a scale of 1:10000 (Fig. 2) and two well preserved frontal moraines, reaching a maximum altitude higher than 1175 m (Entrelagos Moraine) and more than 1000 m in Ercina Lale, have been identified, as previously stated by Alonso (1998). Till is also widespread in the surroundings of Lago Enol, reaching altitudes from 1135 m (N Lago Enol) to 1000 m, although ridge moraines are not as well preserved as in Lago Ercina. The presence of a polished surface define the flow of a glacier to the NW (Bricial glacier), while the Enol Valley (Fig. 2) located at the SW of Lago Enol, would define the flow of a glacier tongue to the NE. According to Jiménez-Sánchez and Farias (2002), the Comeya hollow, was filled by meltwater coming from the Enol-Ercina glacier. Therefore, a glacial front would have existed at about 1030 m (the position of the terminal moraine) (Fig.7a). During this phase the basin of Lago Enol could have been formed by glacial

excavation of the bedrock. The infill of Lago Enol must be younger than the Enol glacier melting and retreat. In fact, the date obtained for the Lago Enol bottom sediments averaging the five dates obtained for Unit 3 is 38,000 yrs BP, younger that the onset of lacustrine sedimentation in Comeya hollow at 43,230 – 45,000 cal yr BP.

The dates obtained from the base of Enol and Comeya deposits (38 to 40 kyr BP) and the geomorphological evidence clearly points to a glacier retreat that started earlier than in other areas of continental ice sheets in North America and North Europe. In addition, it has to be noted that this deglaciation process is also asynchronous with the marine sediment records of global ice volume in which ice volume at 40 kyrs is high and does not start to decrease until 18 kyrs, just after the global LGM (eg. SPECMAP curve in Martinson *et al.*, 1987). Although the causes for the early glacier retreat in the Pyrenees and the Cantabrian Mountains are still not clear (Delmas *et al*., 2008), the chronological model and the Enol record (Fig 6) indicates that the Enol glacier was retreating from 38 till 26 kyr BP and proglacial sediments (Unit 3) were deposited in the Lago Enol basin and the Comeya Hollow. After 26 kyr ago, the environmental situation changed towards sediments slightly enriched in TOC (%), Fe (cps) and MS (Fig. 3 and 4). Thus, from 38 kyr to 26 kyr, Lago Enol behaved as a proglacial lake and, during some intervals, laminated and rhythmite-type sediments (Subfacies 4b) were preserved. Those sediments are interpreted as rhythmites deposited in progracial lakes with a strong seasonality (Leonard and Reasoner, 1999; Ohlendorf *et al.*, 2003): the calcite-rich, coarse silt laminae deposit during the melting season and the fine-grained clay-rich laminae during the winter, when the lake was ice-covered. Coarser laminae deposited during years with stronger pulses of meltwater. Rhythms composed of three laminae could correspond to years with double deposition during the warmer season, one associated with melting water and other to increased precipitation as has been shown in some lakes (Blass *et al*., 2003). In proglacial environments, better development of laminated sediments would occur during periods of stronger seasonality with higher melting and run-off discharges during spring and summer and longer ice-covered winters. More massive Subfacies 4a are finer-grained, clay-rich and with no carbonate. They would deposit during periods with less marked seasonality (colder summers), less available water for runoff when only fine glacial sediment were mobilized ("glacial flour"). Higher carbonate content in Enol proglacial sediments is clearly associated with the coarser sediment fraction.

Sediments from Unit 2, with a slow increase in TOC (%) from 26 kyr to 18 kyr BP, probably are indicating a second step in the glacier retreat that may coincide with the Enol glacier capture by the Bricial glacier represented in Fig.7c. We propose, that the Bricial glacier located at the S of both lakes, captured the main flow of ice from the South of the Massif, accelerating glacial retreat in the Lago Enol catchment (Fig. 7c) and cutting off the lake from any direct glacial influence, as indicated by the presence of a lateral NNW-SSE moraine (Fig. 2). In such hypothetical situation, Lago Enol (not a proglacial lake anymore) would receive less glacial melt water and also it will be under warmer climate with a longer ice-free period. This decreased glacial influence likely favoured the onset of lacustrine biological activity leading to the slight TOC (0-2 %) increase detected along Unit 2 (Facies 3).

The main data from Enol sequence are represented versus age in Fig. 8. The onset of deglaciation inferred from Lago Enol is coherent with El Portalet peatbog, a recently dated sequence in the southern slope of the Pyrenees at 1802 m asl (González-Sampériz *et al*., 2006). The base of this sequence was dated to 33,000 cal yr BP in a pollen concentrate sample, indicating that at that time the Gállego glacier had already retreated at that high altitude. This evidence, together with other dates from several Pyrenean paleoclimate archives, such as lake records (García-Ruíz *et al*., 2003; Jalut *et al*., 1992; Montserrat, 1992), stratified screes (García-Ruíz *et al*., 2001) and fluvial terraces (Sancho-Marcén *et al*., 2003), confirmed that most Pyrenean glaciers on the southern slopes retreated from their maximum extent by 30,000 yr. For the Cantabrian Mountains, our data suggest that by 38,000 yrs Enol glacier was located next to the SW border of Lago Enol (Fig. 7b) and by 26,000 it was farther south, probably not influencing Enol lacustrine sedimentation (Fig. 7c).

During the deposition of Units 3 and 2, only three short intervals with carbonate in the Enol deposits occurred (Fig. 8: 34-30 kyrs; 28.5-27.5 kyrs; ≈22.5 kyrs). In this geological context, the presence of calcite in the sediments would be expected to be dominant since the catchment area is mostly made of limestone (Picos de Europa Formation). However, we need to take into account several factors that would reduce the carbonate presence during OIS 3 and 2: (1) a reduction in the detrital carbonate supply due to frozen soils and scarce water availability in such a cold and dry period,

(2) a reduction in dissolved carbonate due to the low CO_2 dissolved in the waters as a consequence of barren soils in the catchment and (3) longer periods of ice coverage which limit mixing and outgassing of CO_2-rich deep lake waters. It must be noted that groundwater that feeds Lago Enol circulates a short distance and using preferential structural directions (Meléndez Asensio *et al*., 2002). Therefore, the low contact time with the limestone and the expected low dissolution capacity of groundwater may lead to a subsaturated state of bottom waters in Lago Enol. In addition, during OIS 3 and 2 frozen soils would provide an effective barrier against infiltration, thus reducing even more the availability of carbonate-rich groundwater. All the usual factors that are associated with elevated rates of chemical weathering, such as water, soil, and vegetation, would be either entirely absent or absent for much of the year in a glaciated environment. Glaciated regions are largely frozen for significant periods each year, the residence time of liquid water in the catchment is low, there are thin, skeletal soils, and vegetation is either absent or limited (Tranter, 2003). Palynological analyses in Lago Enol sediments (in preparation) indicate very low pollen content in those intervals, thus supporting this hypothesis. In such a situation, the scarce detrital calcite arriving to the Lago Enol will be dissolved particularly the fine-grained fraction, during long periods of ice coverage (Facies 3 and Subfacies 4a). The two intervals with carbonate during the glacial period (Subfacies 4b and 4c) can be interpreted as warmer climate interludes with increased runoff able to supply both enough coarser detrital material and dissolved carbonate to the basin to reach the saturation state, so post-depositional dissolution would be less significant. Shorter periods of ice coverage, with greater overturning, would allow preservation of calcite in saturated bottom waters (Ohlendorf and Sturm, 2001). The occurrence of higher carbonate content associated with laminated and rhythmic intervals suggests relatively warmer summers more conducive to stronger meltwater and sediment inputs to the lake. The first carbonate period appears between Heinrich Event 4 and 3, the second one right after HE 3 and a very short one right after HE2 (Fig. 8). Although the climate conditions during these three intervals were still cold, the evidence given above suggests a slight climatic warming with higher water availability and shorter periods of ice coverage.

The change from glaciolacustrine sedimentation (indicated by laminated sediments and very low organic content that characterize Units 3 and 2) to a more organic sediment (Unit 1) occurred in Lago Enol at 18 kyrs, just after the global LGM (Fig. 8). The first

indication comes from the increase in the TOC (%) followed by the increase in Ca and TIC (%) and decrease in the other elements associated with clays (Fe, Ti, Si, K). This substitution is coherent with the change from Facies 3 (*Gray massive to faintly banded siliciclastic silty-clay with rare biogenic material)* to Facies 1 (*Brown to dark brown, massive to faintly banded carbonatic silts to silty-sand)* (Fig. 3) and certainly represents an environment with more soil development and water availability and, consequently, a probably denser vegetation cover. The much higher carbonate preservation in Lago Enol sediments was facilitated by the warmer climates with wet summers (long ice free periods and more catchment erosion) which provided increased sedimentation rates, as well as more complete lake turnover, CO_2 degassing, and greater groundwater alkalinity fluxes. This transition in Enol sediments occurred in two phases with a stabilization period in between (Fig, 8): (1) from 18 to 14.5 kyr both TIC and TOC rise, (2) from 14.5 to 13.5 kyr values are constant and (3) from 13.5 to 11.5 kyr we observe the final rise towards Holocene values. Although very low LSR that characterized Enol sediments during deglaciation impedes a high resolution reconstruction (Fig. 6), the lake sequence is coherent with the oceanographic changes that occurred in the North Atlantic at that time (eg. Marchitto *et al.*, 2007). The phases of the last deglaciation are:(1) collapse of the North Atlantic Deep Water just after 18 kyr due to a massive discharge of glacial ice and fresh water to the North Atlantic during the HE1; (2) recovery of NADW during the B/A warm phase and (3) another weakening during the YD cold period, probably also triggered by a discharge of glacial meltwater (McManus *et al*., 2004). At 11,500 cal yrs BP, at the onset of Holocene, an increase in TOC and TIC percentages in Lago Enol sediments indicates higher lake level conditions, higher development of soils and increased humidity. Elements associated with clay fraction and siliciclastic supply, such as Fe or Ti, decrease marking the establishment of post-glacial environments in the watershed (Fig. 8). Holocene sediments are interrupted with the presence of slides that may be related to unstable slopes due to the increase in lake level at about 9000 cal yrs BP.

6. Conclusions

The combination of a geomorphological study and the multi-proxy (mostly sedimentological and geochemical indicators) analyses carried out on the lacustrine sequence from Lago Enol have allowed to infer the timing and main phases of the last

deglaciation in the Picos de Europa National Park. Thus, the Enol-Ercina glacial front is reconstructed at about 1030 m asl ≈40,000 yrs ago based on the position of terminal moraines. At that time, Comeya proglacial lake was active and fed by the Enol glacier. After that, the glacier experienced an important and rapid retreat to the headwater of Enol Valley thus forming Enol proglacial lake. These early dates are supporting other observation in southern Europe mountains indicating that last deglaciation took place earlier than in northern Europe. The next sedimentation change recorded in the lake cores coincides with the transition from proglacial Unit 3 to Unit 2 interpreted as a slight warming at 26,000 cal yrs BP. This modification in the environment may be related to the capture of Enol glacier by the Bricial glacier that would have lead to less glacial influence in the Enol catchment area. Along Units 3 and 2, the intervals that have some carbonate preserved coincide with relatively warmer periods in a global climate context (between HE4 and HE3, after HE3 and after HE2).

Finally, the change from glaciolacustrine sedimentation to more organic sediments and more detrital carbonate (represented by Unit 1) is observed in Lago Enol at 18 kyrs, just after the global LGM. In spite of the low sedimentation rate for the interval among the global LGM and the Holocene, it is noted that the transition occurred in two phases with a stabilization period in between, similarly to North Atlantic deglaciation phases during Termination 1. Holocene sediments are characterized by high carbonate and organic matter content pointing to higher lake levels, greater development of soils and increased humidity.

Acknowledgements

This research has been funded through the projects LIMNOCLIBER (REN2003-09130-C02-02), IBERLIMNO (CGL2005-20236-E/CLI), LIMNOCAL (CGL2006-13327-C04-01) and GRACCIE (CSD2007-00067) provided by the Spanish Inter-Ministry Commission of Science and Technology (CICYT). Additional funding was provided by the Spanish National Parks agency through the project "Evolución climática y ambiental del Parque Nacional de Picos de Europa desde el último máximo glaciar - ref: 53/2006" A. Moreno acknowledges the funding from the European Commission's Sixth Framework Program (Marie Curie Outgoing International Fellowships, proposal 021673-IBERABRUPT). We are indebted to Anders Noren, Doug Schnurrenberger and Mark Shapley (LRC-University of Minnesota) for the 2004 coring campaign, Iñaki

Vadillo for his help on water chemistry calculations, Erik Brown (LLO, Duluth, University of Minnesota) for his technical help on the XRF core scanner, Juan R. Bahamonde for his help on the description of the geology of the study area, Vania Stefanova for his help on the age model construction and EEAD-CSIC and IPE-CSIC laboratory staff for their collaboration in this research. Director and staff of the Picos de Europa National Park (PENP) are also acknowledged for their help on the sampling campaigns.

Table captions

Table 1. Sedimentary facies in Lago Enol cores. Mineralogical semi-quantification includes: calcite (cal), clay minerals (cl), quartz (qtz) and feldspars (fd). Grain size distribution is averaged for the analyzed samples corresponding to each facies. Cl=Clay; Si=Silt; Sa=Sand.

Facies	**Description**				
	Physical properties **TIC and TOC content** **XRD mineralogy**	**Grain size distribution**			
		%Clay	%Silt	%Sand	Clay/(Silt+Sand)
Facies 1: Brown to dark brown, massive to faintly banded carbonatic silts to silty-sands.	High MS (≈20 SI); low density; high TIC (4-6%). TOC: 4%. Cal:60-80; Cl: ≈15%; Qz: 10-20%; Fd: ≈5%	37.69	61.61	0.69	0.61
Facies 2: Dark brown mm-thick laminae composed mostly by macrophyte remains	Lower MS than Facies 1 (≈ 15) but similar density; TIC 4-5% and TOC above 8%, mostly terrestrial plants. Cal:60-70; Cl: ≈20%; Qz: 10-20%; Fd: ≈5%	34.04	63.60	2.37	0.52
Facies 3: Grey massive to faintly banded siliciclastic silty-clay with rare biogenic material	Variable magnetic susceptibility (8-20 SI); low density; TIC: very low except one peak reaching 3% in core 2A; TOC: ≈ 0%. Cal:0%; Cl: 40-60%; Qz: 40%; Fd: 10-15%	52.68	47.33	0.00	1.11
Facies 4: Gray mm-thick laminations with siliciclastic clay matrix and common calcitic and quartz crystals in the silt fraction	Relatively low MS (≈ 10) except two peaks in core 1D related to Mn and Fe minerals; high density; TOC and TIC ≈ 0% except on Subunit 3B (TIC= 2-3%). Cal:0-40%; Cl: 20-50%; Qz: 30-40%; Fd: 5-15%	52.93	47.02	0.05	1.19
Facies 5: Carbonate sand with shells fragments (mainly bivalves)	Cm-thick layer only present in core 2A marked by a sharp increase in Ca (not shown), TIC and L*	No data available			

Table 2. Radiocarbon dating of Enol cores analyzed at Poznan Radiocarbon Laboratory, Poland (Poz-) and Lawrence Livermore National Laboratory (Law-). Italic samples belong to the slides (see text for explanation). Last column indicate the calendar age average probability provided by the CALIB software. The ^{14}C date obtained at Comeya basin is also shown (Jiménez Sánchez and Farias, 2002).

Sample	Lab code	Material	Depth (cm)	^{14}C ages	Cal years BP (1-σ)	Calendar age BP
Core ENO04-1D						
ENO04-1D-1K-1- 7	Poz-18434	Bulk sediment	3	2515 ± 35	2501-2595	2590
EN04-1D-1K-1 35	Law-135490	Charcoal	31	5270 ± 60	5986-6029	6060
ENO04-1D-1K-1, 64	Poz-15968	Bulk sediment	60	6660 ± 40	7507-7575	7530
ENO04-1D-1K-1, 95	Law-137659	Charcoal	90	7875 ± 50	8594-8728	8690
ENO04-1D-1K-1, 137	*Poz-12967*	*Bulk sediment*	*133*	*8780 ± 50*	*9697-9900*	9800
ENO04-1D-1K-2- 2	*Poz-18435*	*Plant remains*	*150*	*9050 ± 50*	*10194-10242*	10220
ENO04-1D-1K-2, 12	*Poz-20060*	*Bulk sediment*	*160*	*10560 ± 50*	*12581-12710*	12600
EN04-1D-1K-2 26	*Law-135491*	*Charcoal*	*174*	*15650 ± 380*	*18616-19323*	18910
ENO04-1D-1K-2, 34	*Poz-20061*	*Plant remains*	*182*	*8310± 50*	*9273-9425*	-
ENO04-1D-1K-2, 35	*Poz-12997*	*Bulk sediment*	*183*	*8340± 60*	*9290-9443*	-
EN04-1D-1K-2 49	*Law-135492*	*Charcoal*	*197*	*9870 ± 60*	*11213-11326*	-
ENO04-1D-1K-2- 53	Poz-18436	Bulk sediment	201	16060 ± 80	19122-19354	19240
ENO04-1D-1K-2, 78	Poz-20062	Bulk sediment	226	19190 ± 100	22523-22882	22700
ENO04-1D-1K-2, 128	Poz-16012	Bulk sediment	276	21200 ± 140	25427-25740	25600
ENO04-1D-1K-3- 52	Poz-18456	Bulk sediment	347	32400 ± 700	36853-38729	
ENO04-1D-1K-3, 91	Poz-12251	Bulk sediment	386	31700 ± 500	36225-37829	
ENO04-1D-1K-4, 145	Poz-12252	Bulk sediment	585	32600 ± 500	37151-38727	
Core ENO04-2A						
ENO04-2A-1K-3 55	Poz-25433	Bulk sediment	305	7760 ± 50	8425-8609	8530
ENO04-2A-1K-3 60	Poz-25434	Bulk sediment	310	15870 ± 100	18948-19155	19060
ENO04-2A-1K-3 65	Poz-25435	Bulk sediment	315	17380 ± 110	20350-20909	20520
ENO04-2A-1K-4- 44	Poz-18457	Bulk sediment	439	36200 ± 1100	40023-42250	
ENO04-2A-1K-4- 135	Poz-18458	Bulk sediment	530	32500 ± 500	37065-38689	
Comeya basin						
Onset of lacustrine sedimentation		Organic remains	3500	40880 ± 820	43230–45000	

Table 3. Pearson correlation coefficients among the elements obtained by the ITRAX XRF Core Scanner, the magnetic susceptibility (MS), the lightness (L*) and the percentages of TIC and TOC. Only significant correlations (p-value < 0.01) are shown.

	MS	L*	Si	K	Ca	Ti	V	Cr	Mn	Fe	Rb	Sr	Zr	Ba	Pb	TIC	TOC
MS	1																
L*	-.375	1															
Si	-.348	.759	1														
K	-.449	.757	.944	1													
Ca	.399	-.336	-.622	-.741	1												
Ti	-.457	.707	.910	.981	-.827	1											
V	-.434	.550	.787	.907	-.870	.928	1										
Cr	-.407	.372	.579	.735	-.867	.788	.922	1									
Mn		.452	.247	.259		.227	.120		1								
Fe	-.334	.467	.677	.758	-.903	.828	.796	.764	.264	1							
Rb	-.491	.602	.816	.938	-.895	.967	.966	.877	.121	.837	1						
Sr	-.471	.844	.910	.941	-.606	.921	.773	.595	.343	.677	.833	1					
Zr	-.215	-.123	.112	.229	-.676	.346	.506	.646	-.414	.408	.478		1				
Ba	-.333	.226	.422	.565	-.675	.596	.788	.901		.491	.708	.416	.617	1			
Pb	-.143	.134	.335	.413	-.779	.511	.552	.623	.108	.869	.575	.294	.467	.388	1		
TIC	.434	-.411	-.670	-.768	.958	-.846	-.861	-.848		-.905	-.894	-.661	-.616	-.646	-.763	1	
TOC	.486	-.725	-.816	-.879	.785	-.903	-.829	-.736	-.243	-.845	-.883	-.854	-.299	-.533	-.598	.810	1

Table 4. Principal Component Analyses (PCA). (a) The eigenvalues for the first 14 obtained axes are shown. The percentage of the variance explained by every axis is also indicated. (b) The factorloads for every variable in the two main axes.

(a)

	Axis													
	1	**2**	**3**	**4**	**5**	**6**	**7**	**8**	**9**	**10**	**11**	**12**	**13**	**14**
Eigenvalues	11.46	2.37	1.00	0.85	0.53	0.21	0.18	0.12	0.07	0.05	0.04	0.04	0.03	0.02
Percentage (%)	67.43	13.94	5.86	4.98	3.09	1.26	1.07	0.72	0.43	0.30	0.24	0.21	0.16	0.13
Cum. Percentage	67.43	81.37	87.23	92.21	95.30	96.56	97.62	98.34	98.78	99.07	99.31	99.52	99.67	99.81

(b)

	Axis 1	**Axis 2**
MS	-0.218	-0.156
L	0.191	0.365
Si	0.263	0.216
K	0.280	0.160
Ca	-0.254	0.267
Ti	0.288	0.091
V	0.287	-0.043
Cr	0.265	-0.197
Mn	0.053	0.445
Fe	0.270	-0.044
Rb	0.292	-0.007
Sr	0.258	0.265
Zr	0.135	-0.411
Ba	0.201	-0.275
Pb	0.213	-0.222
TIC	-0.249	0.248
TOC	-0.271	-0.156

Figure captions

Figure 1. Geographical setting and location of cores ENO04-2A-1K and ENO04-1D-1K in Lago Enol. Maps of the Iberian Peninsula and Asturias are shown for location of the study area. Black frame indicates the area where the geomorphological study was carried out (Fig. 2)

Figure 2. Geomorphological map of Lago Enol surroundings, including the spatial distribution of till, moraine ridges and arêtes. Other deposits are also represented, including mainly alluvial, slope and karstic deposits.

Figure 3. Stratigraphic correlation among Enol cores used in this study: ENO04-1D-1K and ENO04-2A-1. Correlation is based on sedimentary facies, magnetic susceptibility (SI units) measured by the high resolution pointer mounted in a GEOTEK MSCL-XYZ and bulk density (g/cm^3) measured by the standard GEOTEK MSCL, lightness values (from black to white, L*) and the percentage of Total Inorganic Carbon (TIC) and Total Organic Carbon (TOC). The available dates are indicated. Vertical scale is in cm.

Figure 4. (A) Downcore X-Ray Fluorescence data (Si, K, Ca, Ti, V, Cr, Mn, Fe, Rb, Sr and Zr) measured by the ITRAX Core Scanner for the Lago Enol sequence. For some elements, the profiles measured by the ICP-OES are shown (K, Ca, Cr, Mn and Fe) in g/kg by black lines with dots. The available dates for that sequence, sedimentological units and facies and x-ray radiograph are also indicated. (B) Correlation plots of K, Ca, Cr, Mn and Fe values measured by the ICP-OES (g/kg) and the ITRAX Core Scanner (cps). Correlation lines and r^2 values are shown.

Figure 5. Principal Components Analyses carried out with the X-Ray Fluorescence data, MS and Lightness and percentages of TOC and TIC from Lago Enol sequence. The arrows represent the variables used for that analysis and the dots mark the position of every sample.

Figure 6. Chronological model of the studied sequence based on mixed effect regression function (Heegaard *et al*., 2005) of calibrated dates (dashed line framed by continuous lines indicating the dating error). Sediments from the observed slide where

replaced to their original position and considered for the age-depth model. Radiocarbon dates obtained in organic remains (charcoal or plant macrorests) are indicated by (M). Averaged linear sedimentation rate (LSR) for each Unit are shown together with the sedimentological Units and climatic intervals.

Figure 7. Tentative evolution of glaciers in Enol area during the last deglaciation, superimposing deduced flow extension (blue) to the DTM; the active lakes surface is given by dark blue colours: a) Glacier pattern at 40,000 yrs BP: the Comeya lake was receiving melting waters from Enol Glacier; it is possible that glacier fronts would have reached previously Comeya hollow, but morphological evidence is not yet clear ; b) Glacier evolution at 38,000 yrs BP: Enol glacier had experimented an important retreat to the headwater of Enol Valley; c) After 38,000 yrs BP: the ice had retreated of the Enol valley, probably captured by the flow of Bricial Glacier. This evolution pattern must be checked with future absolute ages.

Figure 8. Selected data from Enol Lake sequence plotted against age (magnetic susceptibility, lightness, bulk density, Ca, %TIC, %TOC, Fe, Ti and Mn) and compared with the GISP2 core (Grootes and Stuiver, 1997) for the last 40,000 cal yr BP. Gray bands mark main climatic events since last deglaciation.

References

Aguilar C, Nealson KH. 1998. Biogeochemical Cycling of Manganese in Oneida Lake, New York: Whole Lake Studies of Manganese. *Journal of Great Lakes Research* **24:** 93-104.

Alonso V. 1992: *Geomorfología de las cabeceras de los ríos Narcea, Navia y Sil y del Parque Nacional de la Montaña de Covadonga (NO de la Península Ibérica).* Ph. D. Thesis, Universidad de Oviedo 253 pp.

Alonso V. 1998: Covadonga National Park (Western Massif of Picos de Europa, NW Spain): a calcareous deglaciated area. *Trabajos de Geología,* **20**: 167-181.

Alonso JL, Pulgar JA, García-Ramos JC, Barba P. 1996: Tertiary Basins and Alpine Tectonics in the Cantabrian Mountains (NW Spain), In: Friend, P.F. and Dabrio CJ (Eds.): *Tertiary Basins of Spain: Tectonics, climate and sea-level change,* Cambridge University Press, Cambridge, pp. 214-227.

Arnaud F, Revel M, Chapron E, Desmet M, Tribovillard N. 2005. 7200 years of Rhône river flooding activity in Lake Le Bourget, France: a high-resolution sediment record of NW Alps hydrology. *The Holocene* **15:** 420-428.

Bahamonde JR, Merino-Tomé OA, Heredia N. 2007. A Pennsylvanian microbial boundstone-dominated carbonate shelf in a distal foreland margin (Picos de Europa Province, NW Spain). *Sedimentary Geology* **198:** 167–193.

Bard E, Rostek F, Ménot-Combes G. 2004. Radiocarbon calibration beyond 20,000 14C yr B.P. by means of planktonic foraminifera of thr Iberian Margin. *Quaternary Research* **61:** 204-214.

Blass A, Anselmetti F and Ariztegui D. 2003. 60 years of glaciolacustrine sedimentation in Steinsee (Sustenpass, Switzerland) compared with historic events and instrumental meteorological data. *Eclogae geol. Helv*. **96:** (1), S59-S71

Blum P. 1997. Physical properties handbook: a guide to the shipboard measurement of physical properties of deep-sea cores. ODP Tech. Note, 26 [Online]. Available from World Wide Web: <http://www-odp.tamu.edu/publications/tnotes/tn26/INDEX.HTM>.

Chung FH. 1974. Quantitative interpretation of X-ray diffraction patterns of mixtures: II. Adiabatic principles of X-ray diffraction analysis of mixtures. *Journal of Applied Crystallography* **7:** 526-531.

Delmas M, Gunnell Y, Braucher R, Calvet M, Bourlès D. 2008. Exposure age chronology of the last glaciation in the eastern Pyrenees. *Quaternary Research* **69:** 231-241.

Denton GH, Alley RB, Comer GC, Broecker WS. 2005. The role of seasonality in abrupt climate change. *Quaternary Science Reviews* **24:** 1159-1182.

Denton GH, Broecker W, Alley RB. 2006. The mystery interval 17.5 to 14.5 kyrs ago. In *PAGES News*, (Brigham-Grette J, Kull C, Kiefer T, Eds.); pp. 14-16.

Domínguez-Villar D, Wang X, Cheng H, Martín-Chivelet J, Edwards RL. 2008. A high-resolution late Holocene speleothem record from Kaite Cave, northern Spain: $\delta^{18}O$ variability and possible causes. *Quaternary International* **187:** 40-51.

Eusterhues K, Heinrichs H, Schneider J. 2005. Geochemical response on redox fluctuations in Holocene lake sediments, Lake Steisslingen, Southern Germany. *Chemical Geology* **222:** 1-22.

Farias P, Marquínez J, Rodríguez M L. 1990, Geomorfología y origen de la depresión de Comeya (Picos de Europa, Asturias), In: Gutiérrez, M.; Peña, J.L., Lozano, M.V. (Eds.): *Actas de la I Reunión Nacional de Geomorfología*, Instituto de Estudios Turolenses, Teruel, **1**: 91-101.

Farias P, Jiménez Sánchez M, Marquínez J. 1996. Nuevos datos sobre la estratigrafía del relleno cuaternario de la depresión de Comeya (Picos de Europa, Asturias). *Geogaceta*, **20**: (5): 1116-1119.

Flor G. 2004. Morfologías glaciares a cotas bajas en el borde noroccidental del Parque Nacional de los Picos de Europa (Macizo Occidental, Asturias). In: Flor, G. (Ed.): *Actas de la XI Reunión Nacional de Cuaternario*, 59-66.

Florineth D, Schlüchter C. 2000. Alpine evidence for atmospheric circulation patterns in Europe during the Last Glacial Maximum. *Quaternary Research* **54:** 295-308.

Gale SJ, Hoare PG. 1997 The glacial history of the northwest Picos de Europa of Northern Spain. *Z. Geomorph*, **41** (1): 81-96.

García-Ruíz JM, Valero-Garcés BL, González-Sampériz P, Lorente A, Martí-Bono C, Beguería S, Edwards RL. 2001. Stratified screes in the Central Spanish Pyrenees: paleoclimatic implications. *Permafrost and Periglacial Processes* **12:** 233-242.

García-Ruíz JM, Valero-Garcés BL, Martí-Bono C, González-Sampériz P. 2003. Asynchroneity of maximum glacier advances in the central Spanish Pyrenees. *Journal of Quaternary Science* **18:** 61-72.

Gillespie A, Molnar P. 1995. Asynchronous Maximum Advances of Mountain and Continental Glaciers. *Reviews of Geophysics* **33:** 311–364.

González-Sampériz P, Valero-Garcés BL, Moreno A, Jalut G, García-Ruíz JM, Martí-Bono C, Delgado-Huertas A, Navas A, Otto T, Dedoubat J. 2006. Climate variability in the Spanish Pyrenees during the last 30,000 yr revealed by the El Portalet sequence. *Quaternary Research* **66:** 38-52.

Grootes P, Stuiver M. 1997. Oxygen 18/16 variability in Greenland snow and ice with 103-to 105-year time resolution. *Journal of Geophysical Research* **102:** 26455-26470.

Guiter F, Triganon A, Andrieu-Ponel V, Ponel P, Hébrard J-P, Nicoud G, de Beaulieu J-L, Brewer S, Guibal F. 2005. First evidence of "in situ" Eemian sediments on the high plateau of Evian (Northern Alps, France): implications for the chronology of the Last Glaciation. *Quaternary Science Reviews* **24:** 35-47.

Hamilton-Taylor J, Smith EJ, Davison W, Sugiyama M. 2005. Resolving and modeling the effects of Fe and Mn redox cycling on trace metal behaviour in a seasonally anoxic lake. *Geochimica et Cosmochimica Acta* **69:** 1947-1960.

Heegaard E, Birks HJB, Telford RJ. 2005. Relationships between calibrated ages and depth in stratigraphical sequences: an estimation procedure by mixed-effect regression. *The Holocene* **15:** 612-618.

Hernández Pacheco E. 1914. Fenómenos de glaciarismo cuaternario en la Cordillera Cantábrica. *Boletín Real. Sociedad Española de Historia Natural,* **45**: 407-408.

Hughes PD, Woodward JC. 2008. Timing of glaciation in the Mediterranean mountains during the last cold stage. *Journal of Quaternary Science* **23:** 575-588.

Ivy-Ochs S, Kerschner H, Reuther A, Preusser F, Heine K, Maisch M, Kubik PW, Schlüchter C. 2008. Chronology of the last glacial cycle in the European Alps. *Journal of Quaternary Science* **23:** 559-573.

Jalut G, Montserrat J, Fontugne M, Delibrias M, Vilaplana J, Julià R. 1992. Glacial to interglacial vegetation changes in the northern and southern Pyrenees: deglaciation, vegetation cover and chronology. *Quaternary Science Reviews* **11:** 449-480.

Jiménez Sánchez M, Farias P. 2002. New radiometric and geomorphologic evidences of a last glacial maximum older than 18 ka in SW European mountains: the example of Redes Natural Park (Cantabrian Mountains, NW Spain). *Geodinamica Acta* **15:** 93-101.

Jiménez Sánchez M, Ruíz-Zapata MB, Farias P, Dorado-Valiño M, Gil-García MJ, Valdeomillos-Rodríguez A. 2002. Palaeoenvironmental research in Cantabrian Mountains: Redes Natural Park and Comella basin. *In* "Quaternary climatic changes and environmental crises in the Mediterranean Region." (Ruiz Zapata B, Dorado Valiño M, Valdeolmillos Rodríguez A, Gil García MJ, Bardají Azcárate T, Bustamante I, Martínez Mendizábal I, Eds.), pp. 229-240, Alcalá de Henares, Spain.

Leonard EM, Reasoner MA. 1999. A Continuous Holocene Glacial Record Inferred from Proglacial Lake Sediments in Banff National Park, Alberta, Canada. *Quaternary Research* **51:** 1-13.

Lotter AF, Birks HJB. 2003. Holocene sediments of Sägistalsee, a small lake at the present-day tree-line in the Swiss Alps. *Journal of Paleolimnology* **30:** 253-260.

Marchitto TM, Lehman SJ, Ortiz J, Flückiger J, van Geen A. 2007. Marine radiocarbon evidence for the mechanism of deglacial atmospheric CO2 rise. *Science* **316:** 1456-1459.

Marquínez J. 1989 Mapa geológico de la Región del Cuera y los Picos de Europa. *Trabajos de Geología*, **18**: 137-144.

Marquínez J. 1992. Tectónica y relieve en la Cornisa Cantábrica. In: Cearreta A, Ugarte, F (Ed): *The Late Quaternary in the Western Pyrenean Region*, 141-157. Servicio Editorial Universidad del País Vasco.

Marquínez J, Farias P, Felicísimo AM, Villanueva ML, Humara JL, García P, Menéndez R, Jiménez-Sánchez M. 1990. *Geología del Parque Nacional de la Montaña de Covadonga.* Unpublished Report. ICONA. 240 pp.

Marquínez J, Adrados L. 2000. Geología y relieve de los Picos de Europa. *Naturalia Cantabricae* **1:** 3-19.

Martinson DG, Pisias NG, Hays JD, Imbrie J, Moore TC, Shackleton NJ. 1987. Age dating and the orbital theory of the Ice Ages: development of a high-resolution 0 to 300.000-year chronostratigraphy. *Quaternary Research* **27:** 1-29.

McManus J, Francois R, Gherardi JM, Keigwin L, Brown-Leger S. 2004. Collapse and rapid resumption of Atlantic meridional circulation linked to deglacial climate changes. *Nature* **428:** 834-837.

Meléndez Asensio M, Nuño Ortea C, Rebollar Quirós A. 2002. Incidencia de la contaminación antrópica y ganadera en el acuifero cárstico del entorno de Covadonga (Principado de Asturias). *In*

"Presente y futuro del agua subterránea en España y la directiva marco europea." (Hidrogeólogos AId, Ed.), pp. 512. Fundación Centro Internacional de Hidrología Subterránea, Zaragoza.

Miotke FD. 1968. *Karstmorphologische Studien in der glacial überförtem Höhenstufe der Picos de Europa Nordspanien*. Jahrbuch der Geographischen Gesellschaft zu Hannover, **4**, 161 pp.

Montserrat J. 1992. *Evolución glaciar y postglaciar del clima y la vegetación en la vertiente sur del Pirineo: estudio palinológico*. Instituto Pirenaico de EcologÃ-a: Zaragoza.

Moreno A, Giralt S, Valero-Garcés BL, Sáez A, Bao R, Prego R, Pueyo-Mur JJ, González-Sampériz P, Taberner C. 2007. A 14-kyr record from the tropical Andes: the Lago Chungara sequence (18ºS, northern Chilean altiplano). *Quaternary International* **161:** 4-21.

Moreno A, Valero-Garcés BL, González-Sampériz P, Rico M. 2008. Flood response to rainfall variability during the last 2000 years inferred from the Taravilla Lake record (Central Iberian Range, Spain). *Journal of Paleolimnology* **40:** 943-961.

Morford JL, Emerson SR. 1999. The geochemistry of redox sensitive trace metals in sediments. *Geochimica et Cosmochimica Acta* **63:** 1735-1750.

Naughton F, Sánchez-Goñi MF, Desprat S, Turon JL, Duprat J, Malaize B, Joli C, Cortijo E, Drago T, Freitas MC. 2007. Present-day and past (last 25000 years) marine pollen signal off western Iberia. *Marine Micropaleontology* **62:** 91-114.

Obermaier H. 1914. Estudio de los glaciares de los Picos de Europa. *Trabajos Memorias Museo Nacional de Ciencias Naturales*, **9**: 1-42.

Ohlendorf C, Sturm M. 2001. Precipitation and dissolution of calcite in a Swiss high alpine lake. *Arctic, Antarctic and Alpine Research* **33:** 410-417.

Ohlendorf C, Sturm M, Hausmann S. 2003. Natural environmental changes and human impact reflected in sediments of a high alpine lake in Switzerland. *Journal of Paleolimnology* **30:** 297-306.

Pallàs R, Rodés Á, Braucher R, Carcaillet J, Ortuño M, Bordonau J, Bourlès D, Vilaplana J, Masana E, Santanach P. 2006. Late Pleistocene and Holocene glaciation in the Pyrenees: a critical review and new evidence from 10Be exposure ages, south-central Pyrenees. *Quaternary Science Reviews* **25:** 2937-2963

Peinado Lorca M, Rivas-Martínez S. 1987. *La vegetación de España*, 544 pp.

Reimer PJ, Baillie MGL, Bard E, Bayliss A, Beck JW, Bertrand CJH, Blackwell PG, Buck CE, Burr GS, Cutler KB, Damon PE, Edwards RL, Fairbanks RG, Friedrich M, Guilderson TP, Hogg AG, Hughen KA, Kromer B, McCormac G, Manning S, Ramsey CB, Reimer RW, Remmele S, Southon JR, Stuiver M, Talamo S, Taylor FW, van der Plicht J, Weyhenmeyer CE. 2004. IntCal04 Terrestrial Radiocarbon Age Calibration, 0 to 26 Cal Kyr BP. *Radiocarbon* **46:** 1029-1058.

Ruddiman W, McIntyre A. 1981. Oceanic mechanisms for amplification of the 23.000-year ice-volume cycle. *Science* **212:** 617-627.

Sancho-Marcén C, Peña-Monné JL, Lewis C, McDonald E, Rhodes E. 2003. Preliminary dating of glacial and fluvial deposits in the Cinca river Valley (NE Spain): chronological evidences for the Glacial Maximum in the Pyrenees? In *Quaternary Climatic Changes and Environmental Crises in the Mediterranean Region*, (Ruiz-Zapata B, Dorado-Valiño M, Valdeomillos A, Gil-García MJ, Bardají T, Bustamante I, Mendizábal I, Eds.): Alcalá de Henares, Madrid; pp. 169-174.

Santos Alonso R, Marquínez J. 2005. Las formas del lapiaz en el sector norte del Macizo del Cornión, Picos de Europa. *Cuaternario y Geomorfología,* **19**: (1-2): 35-47.

Schnurrenberger DW, Russell JM, Kelts K. 2003. Classification of lacustrine sediments based on sedimentary components. *Journal of Paleolimnology* **29:** 141-154.

Smart PL. 1986 Origin and development of glacio-karst clossed depressions in the Picos de Europa, Spain. *Z. Geomorph. N. F.*, **30**: 423-443.

Tranter M. 2003. Geochemical Weathering in Glacial and Proglacial Environments. In *Treatise on Geochemistry*, (Drever JI, Holland HD, Turekian KK, Eds.). Elsevier,; pp. 189-205.

Trigo RM, Pozo-Vázquez D, Osborne T, Castro-Díez Y, Gómiz-Fortis S, Esteban-Parra MJ. 2004. North Atlantic Oscillation influence on precipitation, river flow and water resources in the Iberian peninsula. *International Journal of Climatology* **24:** 925-944.

Velasco JL, Araujo R, Álvarez M, Colomer M, Baltanás A. 1999. Aportación al conocimiento limnológico de ocho lagos y lagunas de montaña de Asturias (España). *Boletín de la Real Sociedad Española de Historia Natural (Sección Biología)* **95:** 181-191.

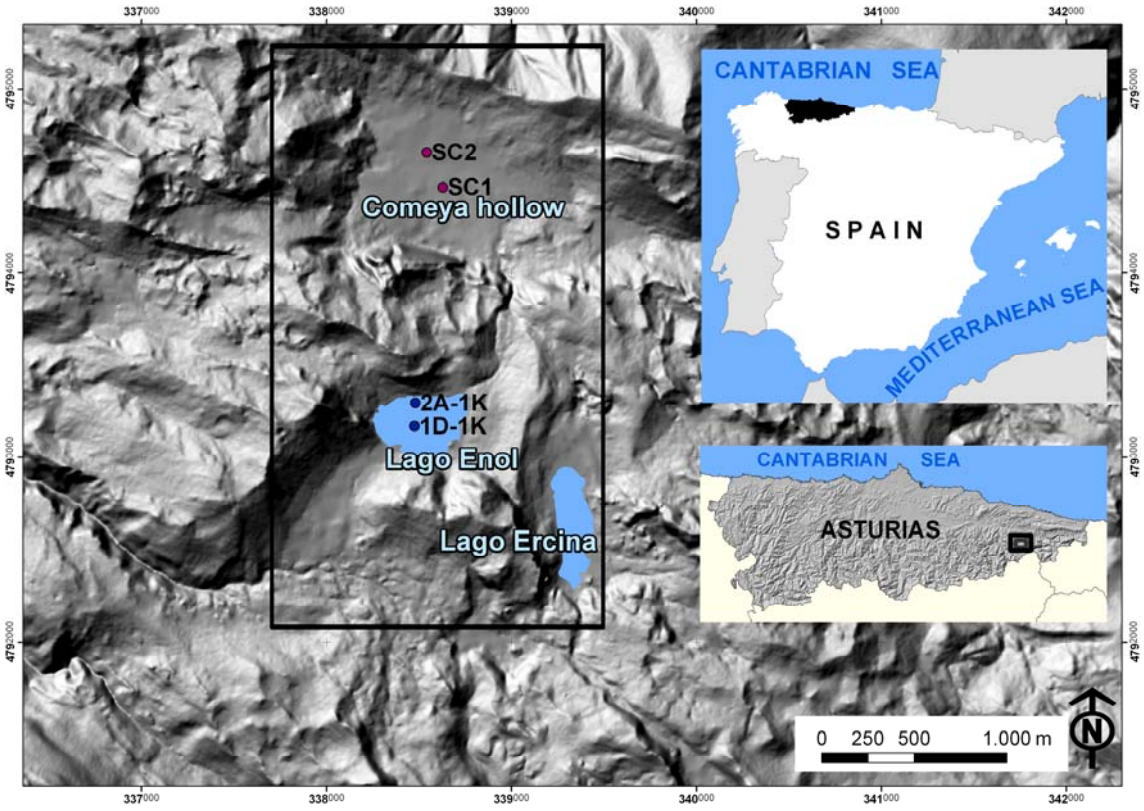
337000
338000
339000
340000
341000
342000
4795000
4794000
4793000
4792000
SC2
SC1
Comeya hollow
2A-1K
1D-1K
Lago Enol
Lago Ercina
CANTABRIAN SEA
SPAIN
MEDITERRANEAN SEA
CANTABRIAN SEA
ASTURIAS
0 250 500 1.000 m
N

FIGURE 1

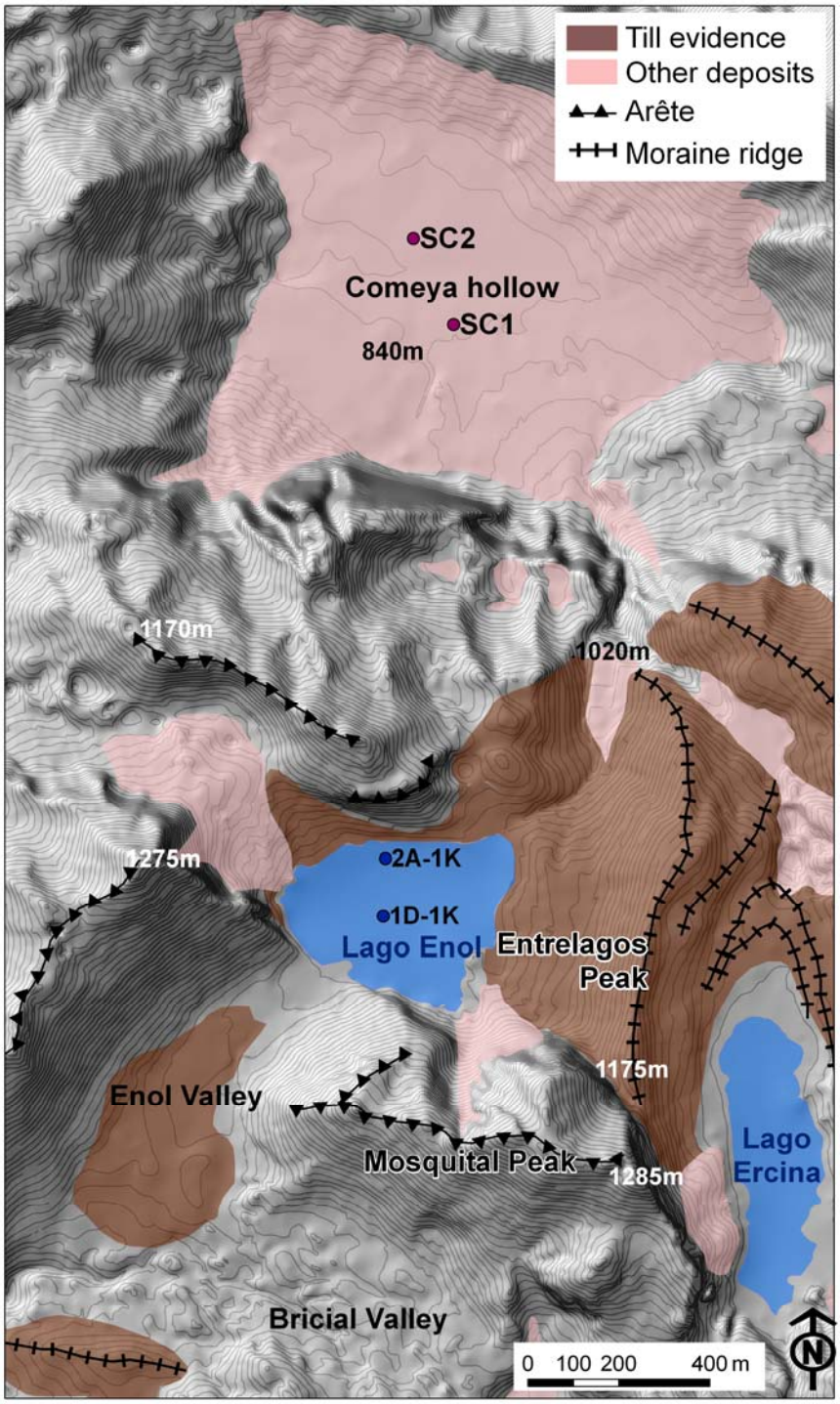
Till evidence
Other deposits
Arête
Moraine ridge
SC2
Comeya hollow
SC1
840m
1170m
1020m
1275m
2A-1K
1D-1K
Lago Enol
Entrelagos
Peak
1175m
Enol Valley
Mosquital Peak
1285m
Lago
Ercina
Bricial Valley
0 100 200 400 m
N

FIGURE 2

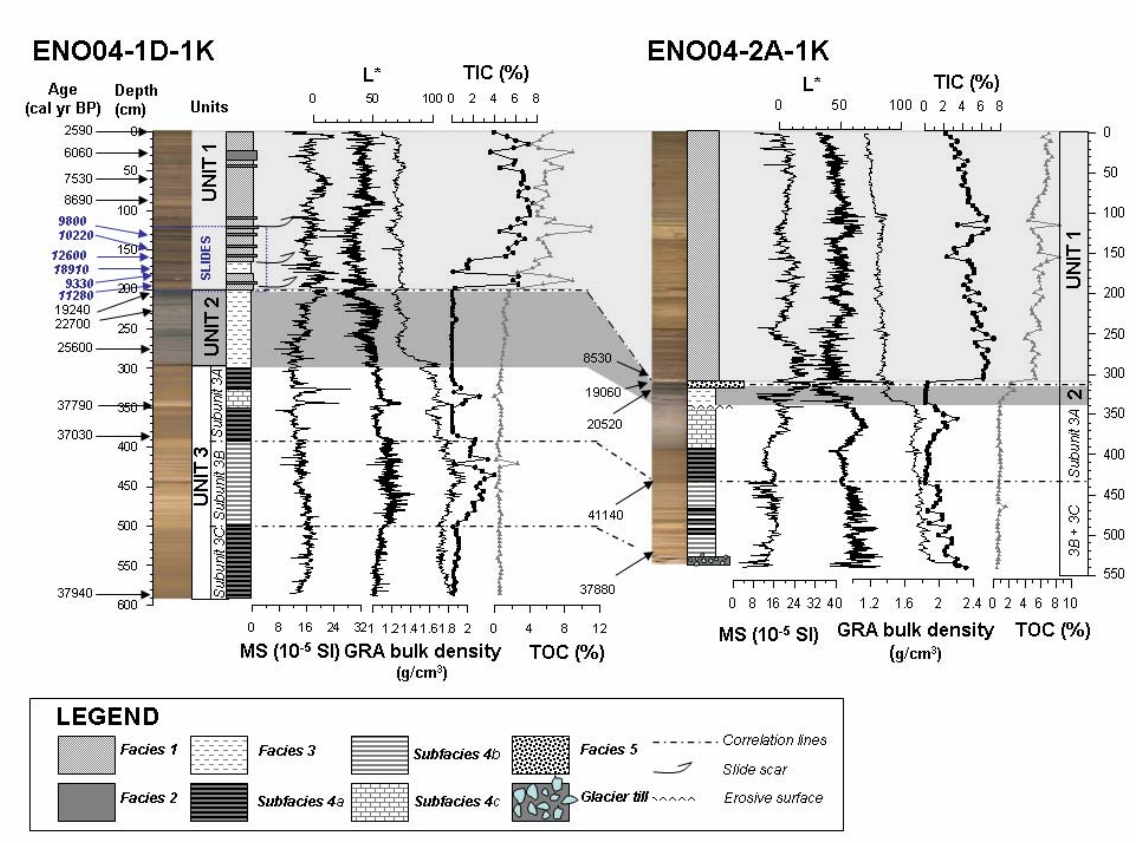
ENO04-1D-1K
ENO04-2A-1K
Age (cal yr BP)
Depth (cm)
Units
L*
TIC (%)
UNIT 1
SLIDES
UNIT 2
UNIT 3
Subunit 3A
Subunit 3B
Subunit 3C
9800
10220
12600
18970
9330
11280
19240
22700
25600
37790
37030
37940
8530
19060
20520
41140
37880
MS (10-5 SI)
GRA bulk density (g/cm3)
TOC (%)
LEGEND
Facies 1
Facies 2
Facies 3
Subfacies 4a
Subfacies 4b
Subfacies 4c
Facies 5
Glacier till
Correlation lines
Slide scar
Erosive surface

FIGURE 3

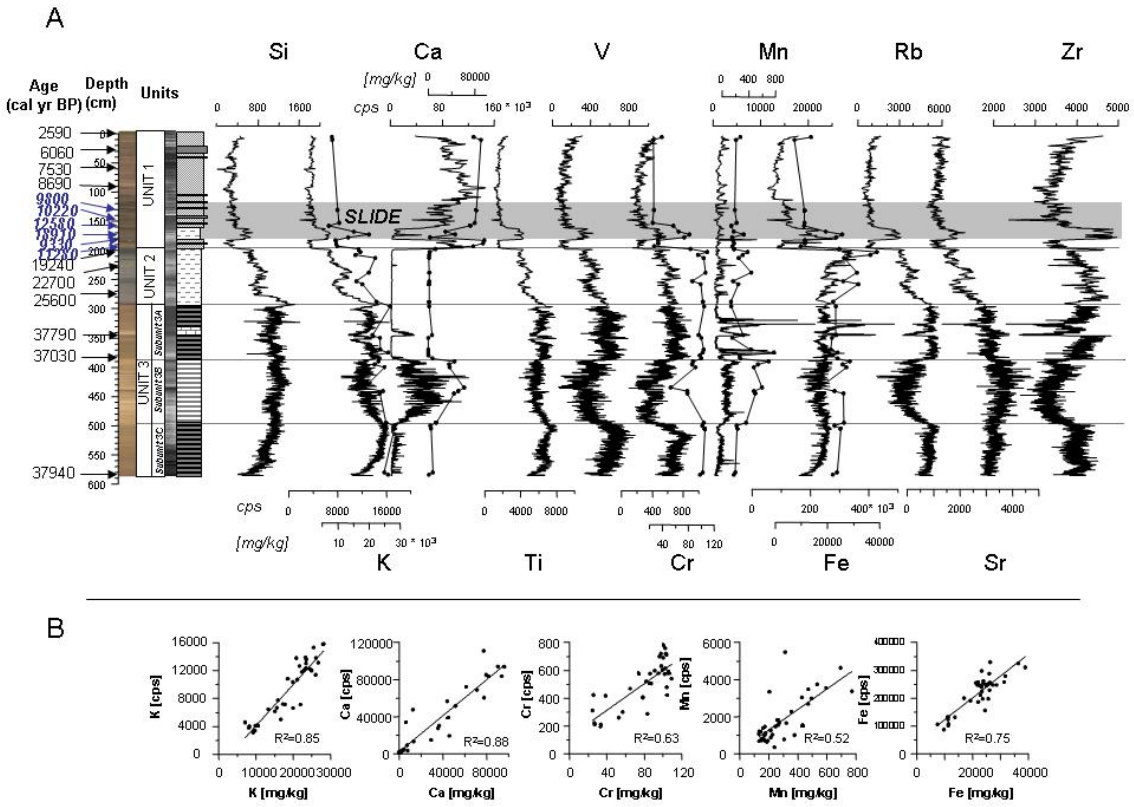
A
Si
Ca
V
Mn
Rb
Zr
Age (cal yr BP)
Depth (cm)
Units
UNIT 1
UNIT 2
UNIT 3
SLIDE
K
Ti
Cr
Fe
Sr
B
R²=0.85
R²=0.88
R²=0.63
R²=0.52
R²=0.75

FIGURE 4

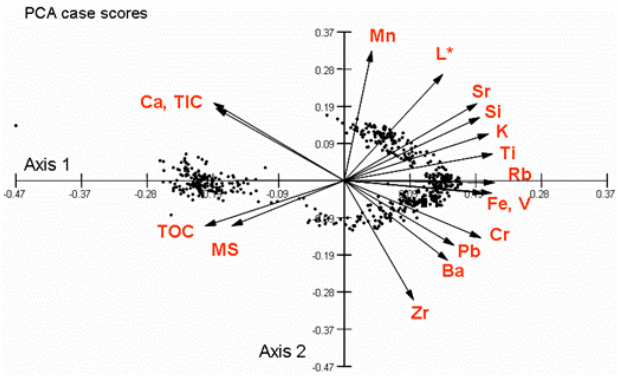
PCA case scores
Mn
L*
Sr
Si
K
Ti
Rb
Fe, V
Cr
Pb
Ba
Zr
Ca, TIC
TOC
MS
Axis 1
Axis 2
0.37
0.28
0.19
0.09
-0.19
-0.28
-0.37
-0.47

FIGURE 5

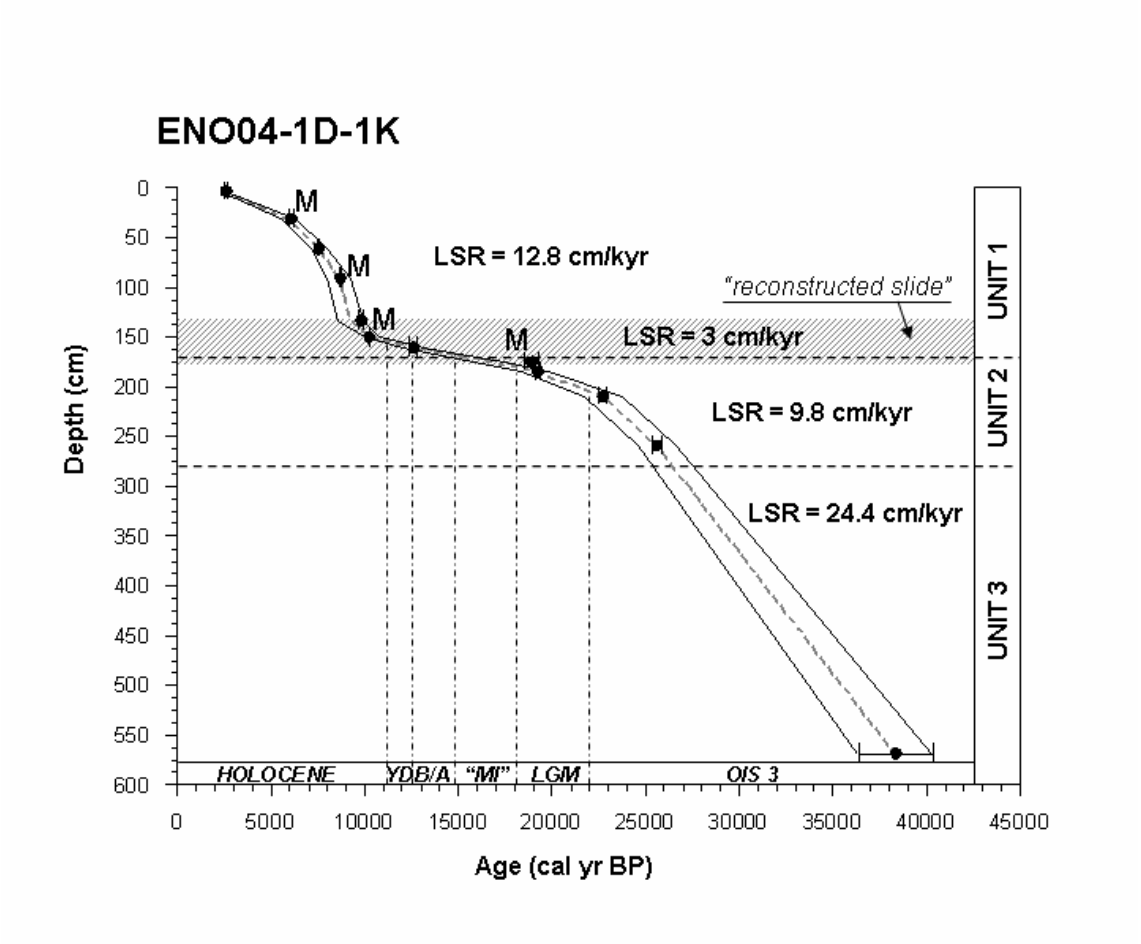
ENO04-1D-1K
Depth (cm)
Age (cal yr BP)
LSR = 12.8 cm/kyr
"reconstructed slide"
LSR = 3 cm/kyr
LSR = 9.8 cm/kyr
LSR = 24.4 cm/kyr
UNIT 1
UNIT 2
UNIT 3
HOLOCENE
YDB/A
"MI"
LGM
OIS 3
M
0
50
100
150
200
250
300
350
400
450
500
550
600
0
5000
10000
15000
20000
25000
30000
35000
40000
45000

FIGURE 6

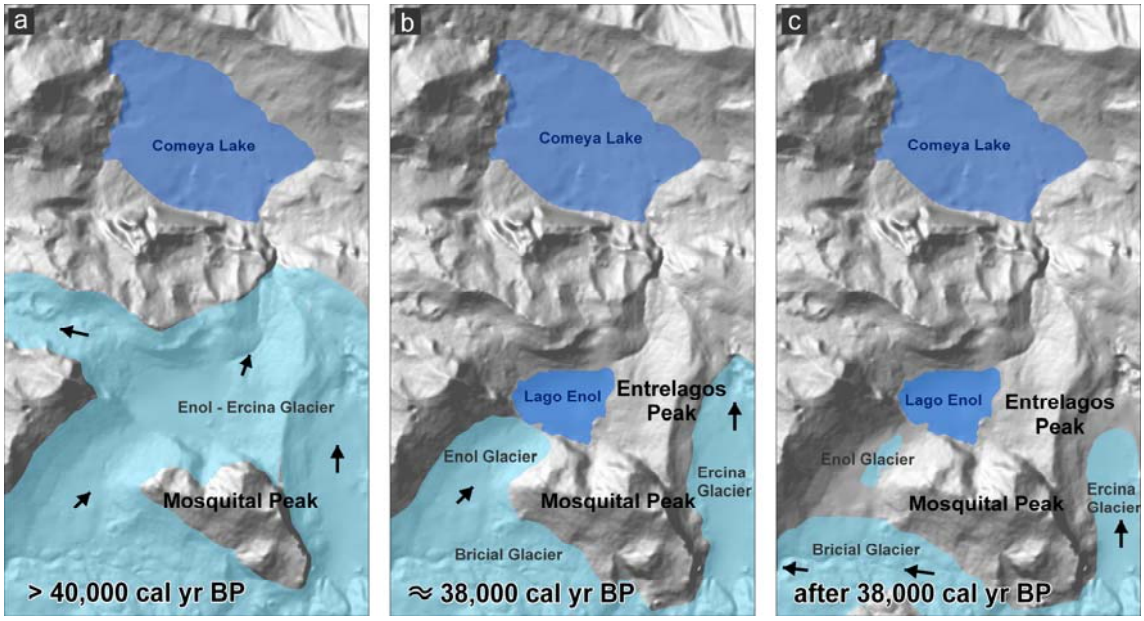
a
Comeya Lake
Enol - Ercina Glacier
Mosquital Peak
> 40,000 cal yr BP
b
Comeya Lake
Lago Enol
Entrelagos Peak
Enol Glacier
Ercina Glacier
Mosquital Peak
Bricial Glacier
≈ 38,000 cal yr BP
c
Comeya Lake
Lago Enol
Entrelagos Peak
Enol Glacier
Ercina Glacier
Mosquital Peak
Bricial Glacier
after 38,000 cal yr BP

FIGURE 7

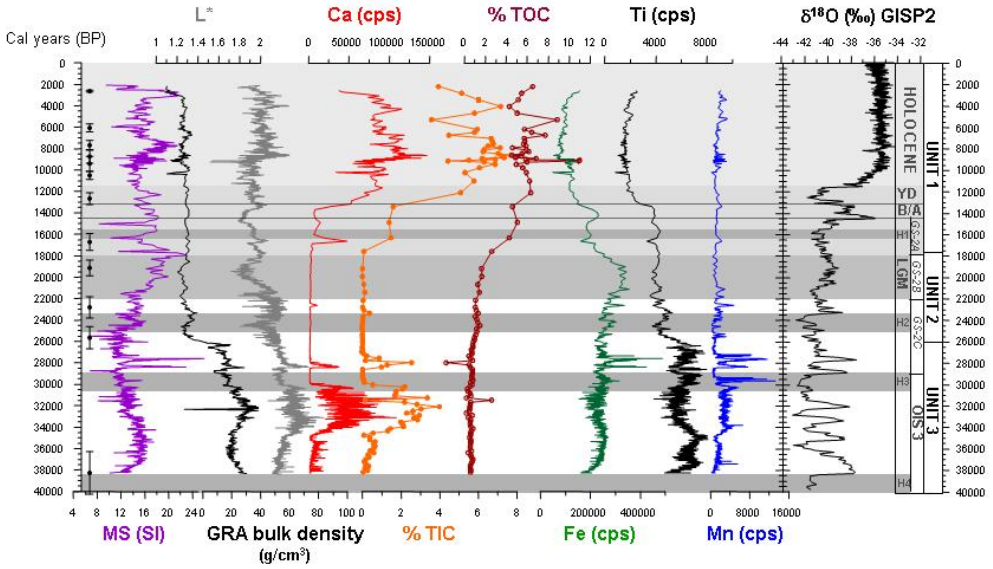
Cal years (BP)
L*
Ca (cps)
% TOC
Ti (cps)
δ18O (‰) GISP2
HOLOCENE
YD
B/A
LGM
H1
H2
H3
H4
UNIT 1
UNIT 2
UNIT 3
GS-2a
GS-2b
GS-2c
OIS 3
MS (SI)
GRA bulk density (g/cm3)
% TIC
Fe (cps)
Mn (cps)

FIGURE 8